TUMOR ANGIOGENESIS, O_2 SATURATION, GLUCOSE AND AMINO ACID METABOLISMS STUDY USING FUNCTIONAL IMAGING

A Dissertation

by

XUEYI XIE

Submitted to the Office of Graduate Studies of
Texas A&M University
in partial fulfillment of the requirements for the degree of

DOCTOR OF PHILOSOPHY

May 2008

Major Subject: Veterinary Pathology

TUMOR ANGIOGENESIS, O_2 SATURATION, GLUCOSE AND AMINO ACID METABOLISMS STUDY USING FUNCTIONAL IMAGING

A Dissertation

by

XUEYI XIE

Submitted to the Office of Graduate Studies of
Texas A&M University
in partial fulfillment of the requirements for the degree of

DOCTOR OF PHILOSOPHY

Approved by:

Chair of Committee,	Georghe Stoica
Committee Members,	Waithaka Mwangi
	Hsin-i Wu
	Suryakant D. Waghela
Head of Department,	Gerald R. Bratton

May 2008

Major Subject: Veterinary Pathology

ABSTRACT

Tumor Angiogenesis, O_2 Saturation, Glucose and Amino Acid Metabolisms Study Using Functional Imaging. (May 2008)

Xueyi Xie, B.S., Qingdao University;

M.S., University of North Texas

Chair of Advisory Committee: Dr. Georghe Stoica

This research is primarily focused on the study of tumors in experimental animal models using functional imaging in the presence of various contrast agents. The study of malignant tumor angiogenesis, oxygen saturation, glucose and amino acid metabolisms will lead to better methods for cancer detection as well as diagnosing and managing cancer. Non invasive *in vivo* diagnostic imaging technique is an area of great clinical interest in present days. In this study, noninvasive *in vivo* photoacoustic tomography and conventional fluorescence imaging together with multiphoton microscopic tomography were implemented to study the malignant tumor morphology and physiology. Tumor structure and angiogenesis were successfully imaged by photoacoustic tomography and conventional fluorescence imaging. The important malignant tumor cellular parameters such as oxygen saturation and $\alpha_v\beta_3$ integrin concentration were measured in living small animals (rodents) using the novel photoacoustic tomography technique. By implementing multiphoton microscopy using Cy3.5 NHS ester contrast agent, tumor amino acid metabolism was successfully studied in cell culture. This method will at least

give you a relative concentration map of amino acid in cells. Non invasive *in vivo* imaging can be achieved by modifying the current multiphoton imaging setup.

A new method for studying amino acid and glucose metabolisms of tumor cells using multiphoton imaging was developed.

ACKNOWLEDGEMENTS

It has been my great pleasure to work in the Veterinary Pathology and Biomedical Engineering departments at Texas A&M University under the supervision of Dr. Gheorghe Stoica for the past few years, which have been the most rewarding experience in my life. I would like to thank Dr. Gheorghe Stoica for giving me the opportunity and supporting me through my research. His broad knowledge and acute insight guided me; his consideration and caring personality inspired me. In his past 25 years life as a professor in Texas A&M University, Dr. Stoica tried his best to advance his students without reservation and gave us plenty of opportunities to communicate with researchers in this field. Without his significant valuable assistance, I would never have been able to successfully complete this research project. He set an excellent example for me both in my future career and personal life.

Last but not least, I would like to thank Dr. Lihong V. Wang, Dr. Hsin-i Wu, Dr. Suryakant D. Waghela, Dr. Waithaka Mwangi, Dr. Alvin T. Yeh, Dr. Xueding Wang, Gina Lungu, Qiaofeng Wu, Dr. Geng Ku and all the people involved in this research for their assistance and contribution to my work.

TABLE OF CONTENTS

CHAPTER Page

LIST OF FIGURES

FIGURE Page

CHAPTER I

INTRODUCTION

Tumor or tumour (via Old French *tumour* from Latin *tumor* "swelling") is an abnormal growth or mass of tissue. A tumor can be either malignant or benign. Nearly all tumors are examples of neoplasia, although certain developmental malformations or inflammatory masses may occasionally be referred to as tumors. Neoplastic tumors are caused by mutations in DNA of cells, which interfere with a cell's ability to regulate and limit cell division. The main focus of this research is using molecular functional imaging to study some of the most important aspects of tumor morphology and physiology.

Molecular imaging is the characterization and measurement of biological processes at the cellular and molecular level in live animals. The study of molecular imaging will lead to better methods for studying complex disease pathways, diagnosing disease at the earliest causative stages. Usually, molecular imaging involves detection of injected exogenous contrast agents such as targeted compounds with fluorescent molecules, radioactive atoms or paramagnetic ions that are visible to the imaging systems. The optical and radiologic imaging modalities such as magnetic resonance imaging (MRI), computed tomography (CT), single photon emission computed tomography (SPECT) and positron emission tomography (PET) have been developed as molecular imaging

---

This dissertation follows the style and format of Optics Letters.

tools for biologist to non-invasively study effects of diseases. Optical imaging techniques have been successfully utilized in whole small animal molecular imaging using near-infrared (NIR) light which can penetrate deeper in the tissue as compared to visible light because NIR light has longer wavelengths, but its high sensitivity and specificity are offset by poor spatial resolution and relatively limited imaging depth. On the contrary, nuclear imaging has the ability to measure radioactivity concentrations with the exquisite sensitivity in deep tissues. However, it involves ionizing radiation whose radioactive decay can't be controlled. In addition, there is always non-specific background signal present in an image due to non-specific binding of radiotracers, residual radiotracer in the circulation and routes of excretion. Photoacoustic imaging technique is utilized to avoid the drawbacks mentioned above.

Tumor angiogenesis is the proliferation of a network of blood vessels that penetrates into cancerous growths, supplying nutrients and oxygen and removing waste products. Tumor angiogenesis actually starts with cancerous tumor cells releasing molecules that send signals to surrounding normal host tissue. This signaling activates certain genes in the host tissue that, in turn, make proteins to encourage growth of new blood vessels.

During the early years, cancer researchers believed that the blood supply reached tumors simply because pre-existing blood vessels dilated. But in 1960's, experiments showed that angiogenesis is necessary for cancerous tumors to keep growing and spreading. This eventually led to the discovery of angiogenesis inhibitors which are used for the cancer

therapy now a day. The imaging of tumor angiogenesis is important for understanding the novel microvessel developing mechanism, monitoring tumor development and angiogenesis inhibitors' therapy effects. The non invasive *in vivo* angiogenesis imaging is achieved through dual modality imaging technique by combining photoacoustic tomography (PAT) and NIR fluorescence imaging in this study as described in chapter II. PAT provides high resolution structural images of tumor angiogenesis, and fluorescence imaging offers high sensitivity to molecular probes for tumor detection. Coregistration of the PAT and fluorescence images was used in this study to visualize tumor location, angiogenesis, and brain structure simultaneously. In U87 tumor, $\alpha_v\beta_3$ integrin is a very important factor for angiogenesis because it functions as a hook to pull out newly developed vessels. Non invasive *in vivo* mapping of tumor $\alpha_v\beta_3$ concentration was achieved and described in chapter IV.

Hypoxia, an imbalance between oxygen (O_2) supply and consumption, is a characteristic feature of locally advanced solid tumors. Major causative factors of tumor hypoxia are abnormal structure and function of the microvessels supplying the tumor, increased diffusion distances between the nutritive blood vessels and the tumor cells, and reduced O_2 transport capacity of the blood due to the presence of disease- or treatment-related anemia. Tumor hypoxia is a therapeutic concern since it can reduce the effectiveness of radiotherapy, some O_2-dependent cytotoxic agents, and photodynamic therapy. Tumor hypoxia can also negatively impact therapeutic outcome by enabling the cells to overcome nutritive deprivation or to escape their hostile environment. The study of

tumor hypoxia will lead to better methods for studying biological processes as well as diagnosing and managing cancer. In chapter III, I present a noninvasive *in vivo* spectroscopic PAT oxygenation measurement technology, which combines high optical contrast with high ultrasonic resolution by employing short laser pulses to generate acoustic waves in biological tissues. Spectroscopic PAT, which is based on the spectroscopic differences among oxygenated hemoglobin and deoxygenated hemoglobin, was successfully used to map the total hemoglobin (HbT) concentration and hemoglobin oxygen saturation (SO_2) in the nude mouse brain intracranial inoculated with U87 glioblastoma tumor cell line which provides direct information related to tumor oxygenation and angiogenesis.

Glucose uptake of malignant glioblastoma tumor can be used to estimate the overall metabolic activity since glucose is the primary energy source. It is a very useful factor for cancer detection, therapy design and treatment monitoring. In chapter V, fluorescent 2-deoxyglucose analog, 2-[N-(7-nitrobenz-2-oxa-1,3-diaxol-4-yl)amino]-2-deoxyglucose (2-NBDG) was used in multiphoton and conventional fluorescence imaging for assessing glucose uptake by U87 glioblastoma cells in *in vitro* culture and U87 tumors xenografted into mice respectively.

By virtue of tumor cell enzymes, neoplastic cells can irreversibly drain the host of essential amino acids. In chapter VI, amino acid metabolism is evaluated by using free amino acid targeting contrast agent Cy 3.5 NHS ester through monitoring the free amino

acid concentration. The tumor-bearing animals are in negative energy balance but in overall positive nitrogen balance due to the growth of the tumor. They decreased their food intake, the energy for the tumor growth is coming from consume body lipids. The nitrogen, which was necessary for the proliferation of the tumor, was made available by a net breakdown of skeletal muscles. The monitoring amino acid metabolism is very important for early cancer detection and future therapy approach. For example, folate (One-carbon amino acid) anti-metabolites such as methotrexate were decided to be used in cancer chemotherapy after the study of amino acid metabolism. The malignant tumor has high rate of proliferation, and hence a high requirement for folate for DNA synthesis, but has only very limited reserves. Therefore it is susceptible to the actions of anti-metabolites. Alternating therapy with folate anti-metabolites, followed by repletion with massive doses of folate, seems to be effective in many cases. In chapter VI, a preliminary method to evaluate fast amino acid metabolism by studying free amino acid is presented. Multiphoton excitation microscopy with the presence of Cy3.5 N-hydroxysuccinimide (NHS) ester contrast agent has a potential to be used for non invasive *in vivo* detection for free amino acid metabolism, at least in small animals.

CHAPTER II

TUMOR STRUCTURE AND ANGIOGENESIS

Overview

Here I present a dual modality imaging technique by combining photoacoustic tomography (PAT) and near-infrared (NIR) fluorescence imaging for the study of tumor in animal model. PAT provides high resolution structural images of tumor angiogenesis, and fluorescence imaging offers high sensitivity with the use of molecular probes for tumor detection. Coregistration of the PAT and fluorescence images was performed on nude mice with subcutaneous M21 human melanoma cells that express $\alpha_v\beta_3$ integrin expression. An integrin $\alpha_v\beta_3$–targeted peptide–ICG conjugated NIR fluorescent contrast agent was used as the molecular probe for tumor detection. PAT was employed for noninvasive imaging the brain structures and the angiogenesis associated with tumors. Coregistration of the PAT and fluorescence images was used in this study to visualize tumor location, angiogenesis, and brain structure simultaneously.

Introduction

The development of noninvasive diagnostic imaging techniques is an area of great clinical interest. Such imaging tools are critical for the study of tumor detection and

physiology, such as tumor angiogenesis. Photoacoustic tomography (PAT) and near-infrared (NIR) fluorescence imaging are noninvasive techniques can detect tumors and provide complementary structural information about angiogenesis. PAT is an emerging imaging modality that takes advantage of both high optical contrast and good ultrasound resolution[1]. Photoacoustic signals are induced by pulsed light illumination. When light energy is absorbed by biological tissues, the resulting thermal expansion of the tissues generates ultrasonic waves that are detected by an ultrasonic transducer for reconstruction of optical absorption distribution inside the tissues. PAT has been shown to be a promising tool for biomedical applications, such as the monitoring of oxygenation in blood vessels, epidermal melanin measurement, angiography, and breast tumor detection[2].

In the conventional fluorescence tomography, the efficient light-emitting process is triggered by the absorption of the excitation radiation of an appropriate wavelength. The fluorescence signal emitted by a molecule or atom after optical excitation can be easily detected even in very low concentrations. Light energy is 'packaged' into discreet bundles called photons. After fluorophores absorb light of certain wavelengths, their electrons transform into an unstable exited state then rapidly lose excess energy and emit light. Proper optical filters can be used to distinguish the excitation and emission lights since the energy of the emitted light is smaller than the absorbed light which means longer wavelength and different color.

Fluorescence imaging has high sensitivity, and can also be used to image a variety of molecular properties due to its versatile fluorescent probe design[3,4]. Fluorescence imaging shows strong potential for the diagnostic imaging of tumors. Recently, Li and Ke et al. developed an integrin $\alpha_v\beta_3$–targeted peptide conjugated with indocyanine green (ICG) as a fluorescent molecular imaging contrast agent for the noninvasive *in vivo* visualization of M21 human melanoma tumors with $\alpha_v\beta_3$ integrin expression. Integrin $\alpha_v\beta_3$ plays an important role in tumor angiogenesis and metastasis.[5,6] This contrast agent was successfully used to identify the M21 tumor in this study due to its $\alpha_v\beta_3$ targeting ability.

Material and Methods

Photoacoustic tomography

The experimental setup for the *in vivo* PAT of a nude mouse is shown in Fig. 1. A tunable Ti:Sa nanosecond pulse laser (LT–2211A, Lotis T II, Minsk, Belarus) pumped by an Nd:YAG laser (LS–2137/2, Lotis T II, Minsk, Belarus) was employed to provide laser pulses with a pulse repetition rate of 10 Hz and a wavelength of 785 nm. The incident energy density of the laser beam on the surface of the mouse head was controlled to < 2 mJ/cm^2. An unfocused ultrasonic transducer (XMS–310, Panametrics) with an active element of 2 mm in diameter, a center frequency of 10.4 MHz, and a -6dB fractional bandwidth of 100% was used to detect the photoacoustic signals. A computer–controlled step motor drove the transducer to circularly scan the cortical surface of the

mouse brain with a radius of 3.5 cm and a step size of 1.5°. The data acquisition time for one image was ~15 minutes. The mouse was fixed by a homemade mount with its head protruding into the water tank through a hole in the bottom of the water tank. The hole was sealed with a piece of polyethylene membrane. The mouse head surface was covered with a thin layer of ultrasonic coupling gel. The detected photoacoustic signals were amplified and then digitized by an oscilloscope. The digitized signals were transferred to a computer, and the distribution of the optical absorption in the imaging plane (x-y plane) was reconstructed using a modified back-projection algorithm after a full view scanning.

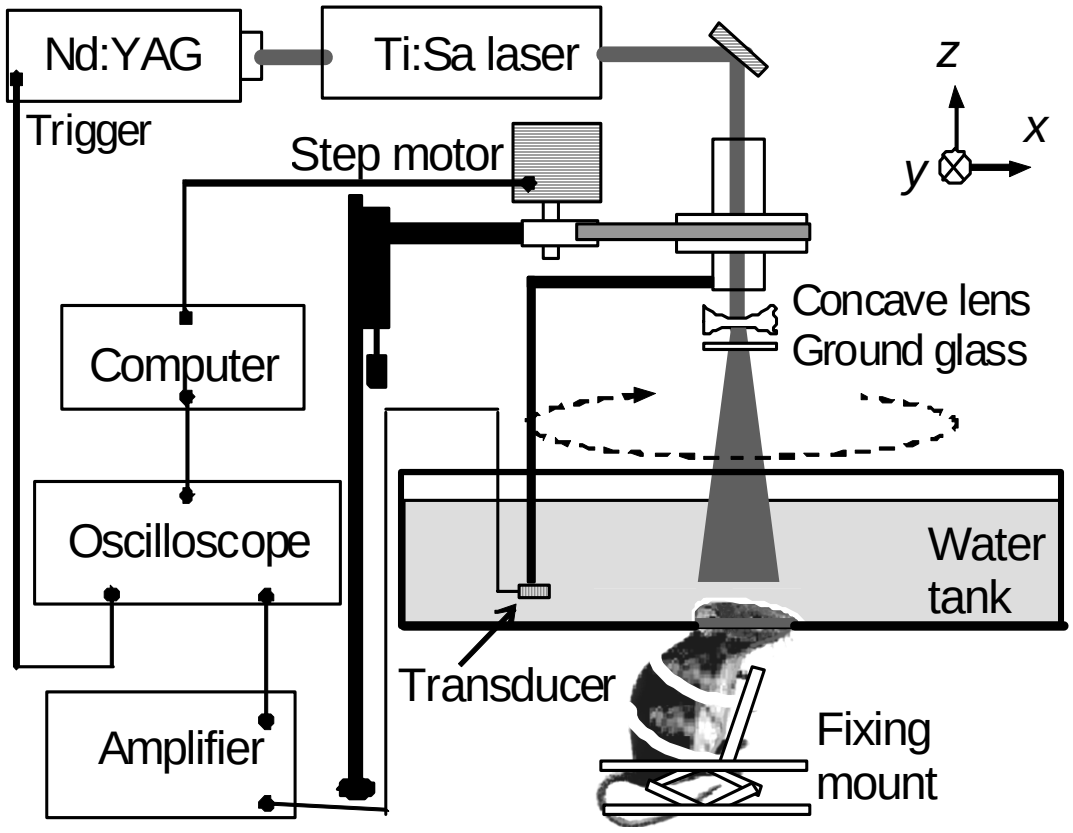

Figure 1. Experimental setup of *in vivo* photoacoustic tomography.

Near-infrared fluorescence imaging

Fig. 2 shows the *in vivo* fluorescence imaging setup for nude mice with a peptide-ICG contrast agent. The mouse head was illuminated with light from a laser diode (785 nm, 80mW) expanded to ~5 cm diameter circular area. A macro lens, coupled to a cooled CCD camera (BU401–BR, Andor Technology, CT), collected the emitted fluorescent light from the conjugated ICG molecules. The lens was fitted with a holographic notch–plus filter (785–nm center wavelength, Kaiser Optical Systems, Inc., Ann Arbor, MI) and a bandpass filter (830–nm center wavelength).

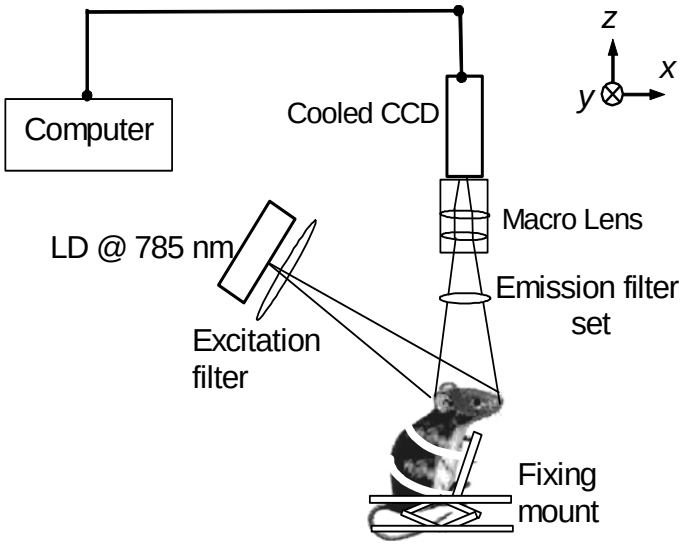

Figure 2. Experimental setup of *in vivo* fluorescence imaging of nude mice with peptide–ICG contrast agent.

Cell culture and animal protocols

All the performed experimental procedures on the M21 tumor cells and mice were approved by the University Laboratory Animal Care Committee of Texas A&M

University and followed the guidelines of the Guide for the Care and Use of Laboratory Animals prepared by the United States National Institutes of Health.

The M21 tumor cell line was maintained in Dulbecco's modified Eagle's medium (DMEM) (Invitrogen, Carlsbad, CA, USA), supplemented with 10% fetal bovine serum (Invitrogen) and antibiotics (100 units/ml penicillin and 100 μg/ml streptomycin).

Nude mice weighing about 20 grams were used for in vivo animal experiments. A dose of 87 mg/kg Ketamine plus Xylasine 13 mg/kg, administered intramuscularly, was used to anesthetize the mice during the experiments. M21 human melanoma tumor cells were inoculated subcutaneously on the head of the nude mice. When the tumor grew to a size of about 5 mm diameter, the peptide–ICG conjugated contrast agent was injected, with an estimated dosage of 10 μM, into the circulatory system of the mice via tail vein injection. The fluorescence and PAT imaging were conducted when the contrast agent cleared from blood circulation system which is about 24 hours after the ICG based contrast agent injection.

Results and Discussion

Fig. 3(a) shows the NIR fluorescent image of a nude mouse inoculated with a M21 human melanoma tumor and injected with an integrin $\alpha v\beta_3$–targeted peptide–ICG conjugated contrast agent. The signal intensity of the tumor region was significantly

higher than that of background due to the uptake of the contrast agent by the $\alpha v\beta_3$ integrin receptors. This fluorescence image shows the location and shape of the tumor.

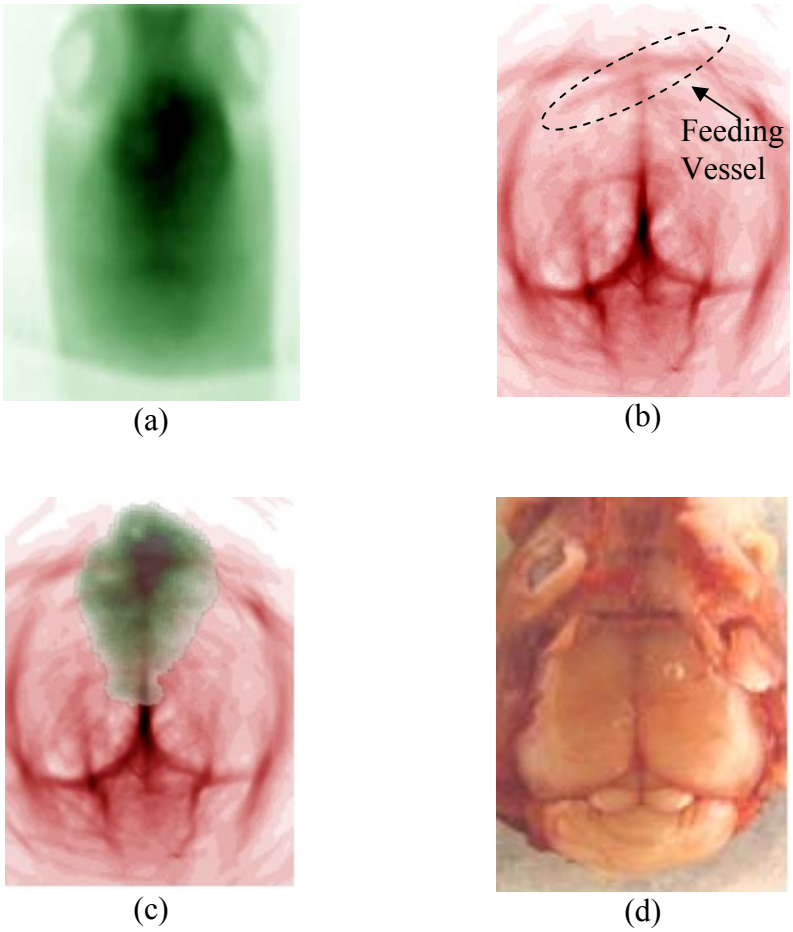

Figure 3. Tumor detection and tumor angiogenesis imaging results.

(a) Noninvasive *in vivo* fluorescence image acquired 24 hours after the ICG injection. (b) Noninvasive *in vivo* PAT image acquired 24 hours after the ICG injection with skin and skull intact. (c) Coregistrated noninvasive *in vivo* image of PAT and fluorescence imaging. (d) Open skin and removed skull photograph.

Fig. 3(b) is the PAT image. It clearly shows the brain surface vascular system of the nude mouse and the structure of the brain. In this experiment, the mouse was fixed on the same mount for both the PAT and fluorescence imaging, and the fluorescence images were acquired from the top of the mouse head in both cases. Hence, the coregistration between the PAT images and fluorescence images is feasible. The coregistered image of the PAT and fluorescence imaging is shown in Fig. 3(c). The fluorescence image was overlapped on top of the PAT image. Comparing Fig. 3(b) with the open skull photograph, Fig. 3(d), we find that the brain structure is well matched except for the dashed circled vessel in Fig. 3(b), which is not shown on the surface of the brain. Based on the coregistrated image, the vessel marked in Fig. 3(b) is one of the major feeding vessels of the tumor.

Conclusion

A dual modality imaging method combining PAT and molecular fluorescence imaging is successfully employed to image the angiogenesis of the brain containing a tumor and to detect the tumor. A tumor-targeted NIR fluorescent contrast agent is used for the tumor detection. By employing coregistration of PAT and fluorescence imaging, the tumor location, the tumor angiogenesis, and the brain structure of the nude mouse can be visualized at the same time. Future work will focus on molecular PAT imaging using spectral information derived from intrinsic and extrinsic molecular contrast.

CHAPTER III

TUMOR SO_2 AND HBT DISTRIBUTION MAPPING

Overview

Hypoxia is important in tumor biology and therapy. The study of tumor hypoxia will lead to better methods for studying biological processes as well as diagnosing and managing cancer. Here we present a noninvasive *in vivo* spectroscopic photoacoustic tomography (PAT) based oxygenation measurement technology, which combines high optical contrast and high ultrasonic resolution by employing short laser pulses to generate acoustic waves in biological tissues. Spectroscopic PAT, which is based on the spectroscopic differences among oxygenated hemoglobin and deoxygenated hemoglobin, can be used to map the total hemoglobin (HbT) concentration and hemoglobin oxygen saturation (SO_2) in the nude mouse brain intracranial inoculated with U87 glioblastoma tumor cells which provides direct information related to tumor oxygenation and angiogenesis.

Introduction

The brain is notable in its dependence on the blood for its immediate supply of oxygen and essential energy substrates. There is a short supply and low levels stored of essential

substrates in the brain, this is a very hypoxia vulnerable organ. An interruption in their delivery leads within minutes to irreversible changes resulting in cell death. The brain is an organ of high metabolic rate and it is largely dependent on the blood to supply the essential fuels for its intense activities. There are clear differences between the in vivo metabolic rates of the brains of different mammalian species. Values for cerebral oxygen and glucose consumption (the cerebral metabolic rate) in the rat are twice those for the dog and three times the values for humans. These data demonstrate the existence of an inverse ratio between brain oxygen consumption and body weight that is probably due to the relative high neuron-packing density and higher neuron-to-glia ratio in the brain of smaller animals.

Cerebral blood oxygenation changes resulting from brain activation are crucial to understanding the mechanism of functional cerebral metabolism and pathophysiology. Tissue hypoxia occurs where there is an imbalance between oxygen supply and consumption. Hypoxia occurs in various pathological conditions including solid tumors as a result of an inadequate supply of oxygen, due to exponential cellular proliferation and an inefficient vascular supply.

Hypoxia is very important in tumor biology and therapy. Hypoxia inhibits cell reproducing and even induces cell death, but it also provides angiogenic and metastatic signals which allow prolonged survival in the absence of oxygen and generation of a persistent angiogenic signal. Hypoxia stimulates tumor cells' production of acids; the

hypoxia and acidity of tumors have important consequences for anti-tumor therapy and can contribute to the progression of tumors to a more aggressive metastatic phenotype. Recently tumor hypoxia in the malignant potential of cancer cells also has been recognized as a physiological stress at a cellular level leading to gene expression in normal and tumor tissue.[7, 8, 9] Consequently, development of a tumour in the brain with demonstrated hypoxia will complicate any therapeutic approach and could result in severe impairment of the normal brain homeostasis with negative effects on the host.

The following are samples of the several non-invasive methods currently available for measure the oxygenation status of a tumor after decades of efforts. Contrast enhanced dynamic computerized tomography (CT)-determined tumor perfusion requires contrast agent and cannot provide the most accurate estimate of tumor oxygenation.[10, 11] Electron paramagnetic resonance (EPR) spectroscopy and imaging techniques have been used to determine oxygenation status of tumors 10 mm from the surface of body by using low molecular weight stable nitroxide free radical probes which have not yet been fully tested in human patients. There are some confounding factors in this method, such as the rate of infusion of the probe into the tumor, metabolic reduction of the probe within tumor tissue and the clearance of the probe from the tumor tissue by blood flow, etc..[12, 13, 14] Oxygen dependent quenching of phosphorescence is another non-invasive optical method for measuring oxygen pressure in tissues. However, this method needs to employ phosphors which have not been used in the clinic in human patients and it is difficult to obtain a good signal-to-noise-ratio. Since the tumor has a relatively leakier

blood vascular system than normal tissue, tumor specific vascular properties will interfere with accuracy of tumor oxygenation measurement.[15] Oxygen saturation can also be measured non-invasively by diffuse light spectroscopy utilizing near-infrared (NIR) absorption spectroscopy to measure tissue absorption at two different wavelengths. The resolution and accuracy is limited by the light scattering in biological tissues while imaging the brain through the intact skin and skull.[16, 17]

Compare to the above methods, PAT has the ability to image hemoglobin concentration and oxygenation simultaneously with high spatial resolution [18] and satisfactory penetration depth (~ 5cm)[19] in the small animal brain with tumor without using contrast agents. Photoacoustic tomography (PAT), employing short laser pulses to generate acoustic waves in biological tissues, overcomes both the resolution disadvantage of optical imaging and the contrast disadvantages of ultrasonography.[20] Spectroscopic PAT of imaging the HbT concentration and hemoglobin SO_2 in the nude mouse brain implanted with human tumor xenograft U87 glioblastoma tumor cell line relies on the spectroscopic differences between oxygenated hemoglobin (HbO_2) and deoxygenated hemoglobin (Hb). In theory, PAT measurements at two wavelengths are sufficient for an absolute estimation of brain oxygenation and a relative estimation of blood volume since HbO_2 and Hb are the dominant absorbers in the mouse brain in the near-infrared (NIR) spectral region under study. In order to increase the accuracy of the measurement, four wavelengths within the range of 764nm to 824nm are used to make the PAT brain SO_2 measurement overdetermined. Within this range, the penetration depth of light in this

range is greater than the size of the imaged brain vessel branches (<50 μm). Meanwhile, Hb and HbO_2 are the only significant absorbers and scattering was assumed to be constant.

Material and Methods

Spectroscopic PAT of HbT and SO_2

Here we explain the principle of spectroscopic PAT using wavelength λ_i within the NIR spectra range. The tissue absorption coefficient $\mu_a(\lambda_i)$ (cm^{-1}) can be expressed as

$$\mu_a(\lambda_i) = \varepsilon_{\mathrm{Hb}}(\lambda_i)[\mathrm{Hb}] + \varepsilon_{\mathrm{HbO_2}}(\lambda_i)[\mathrm{HbO_2}]$$

where $\varepsilon_{\mathrm{Hb}}(\lambda_i)$ and $\varepsilon_{\mathrm{HbO_2}}(\lambda_i)$ are the known molar extinction coefficients (cm^{-1} M^{-1}) of Hb and HbO_2 at wavelength λ_i, respectively;[21] and $[\mathrm{Hb}]$ and $[\mathrm{HbO_2}]$ are the concentrations of the two forms of hemoglobin, respectively. Given that the acquired localized PA signal $\phi(\lambda_i, x, y)$ is linearly related to the voxel's absorption coefficient after being normalized by the tissue's optical wavelength-dependent attenuation and the incident light energy, one can replace the $\mu_a(\lambda_i)$ by $\phi(\lambda_1, x, y)$ to calculate the [Hb] and [HbO_2] under multiple wavelength measurements. In principle, two wavelengths are enough to determine SO_2 from the detected optical absorptions.[22] But in order to reduce the influence of measurement errors, we used four wavelengths in all of our studies. After acquiring the necessary spectroscopic information, least-square fitting gives:

$$\begin{bmatrix} [\mathrm{Hb}] \\ [\mathrm{HbO2}] \end{bmatrix}_{(x,y)} = \left(M^T M\right)^{1} M^T \Phi(x,y), \quad (2)$$

where $M = \begin{bmatrix} \varepsilon_{\mathrm{Hb}}(\lambda_1) & \varepsilon_{\mathrm{HbO2}}(\lambda_1) \\ \vdots & \vdots \\ \varepsilon_{\mathrm{Hb}}(\lambda_n) & \varepsilon^{\lambda_n}_{\mathrm{HbO2}}(\lambda_n) \end{bmatrix}$; and $\Phi(x,y) = \begin{bmatrix} \phi(\lambda_1, x, y) \\ \vdots \\ \phi(\lambda_n, x, y) \end{bmatrix}$.

The point-by-point SO_2 image is therefore calculated as

$$\mathrm{SO}_2 = \frac{[\mathrm{HbO}_2]}{[\mathrm{HbO}_2] + [\mathrm{Hb}]}$$

$[\mathrm{Hb}]$ and $[\mathrm{HbO}_2]$ are the molar concentrations of deoxygenated hemoglobin and oxygenated hemoglobin, respectively.

Experiment setup

The experimental setup for the *in vivo* PAT of a nude mouse head is shown in Fig. 4. A tuneable Ti:Sa nanosecond pulse laser (LT–2211A, Lotis T II, Minsk, Belarus) pumped by an Nd:YAG laser (LS–2137/2, Lotis T II, Minsk, Belarus) was employed to provide laser pulses with a pulse repetition rate of 10 Hz. The laser beam is expanded by a concave lens and homogenized by a ground glass and then is delivered to the animal head. The incident energy density of the laser beam on the surface of the mouse head was controlled to < 3 mJ/cm^2 (within the ANSI standard). Each laser pulse's energy was monitored using photodiode (PD) and recorded for normalizing the photoacoustic signal. An unfocused ultrasonic transducer (V310/2.25MHz, Panametrics) with 6mm active area in diameter is used as the detector to receive the induced acoustic signals. This commercial transducer has nominal bandwidths of 50% to 80% of their central

frequencies. A computer–controlled step motor drives the transducer to circularly scan 3mm below the cortical surface of the nude mouse brain with a radius of 3.5 cm and a step size of 3^{o}. 764nm, 784nm, 804nm and 824nm four wavelengths were implemented in each scanning step. The mouse is fixed by a homemade restrain mount with its head protruding into the water tank through a hole in the bottom of the water tank. The hole was sealed with a piece of polyethylene membrane. The mouse head surface is covered with a thin layer of ultrasonic coupling gel. The detected photoacoustic signals were amplified and then digitized by an oscilloscope. The digitized signals are transferred to a computer, and the distribution of the optical absorption in the imaging plane (x-y plane) is reconstructed using a modified back-projection algorithm after a full view scanning.

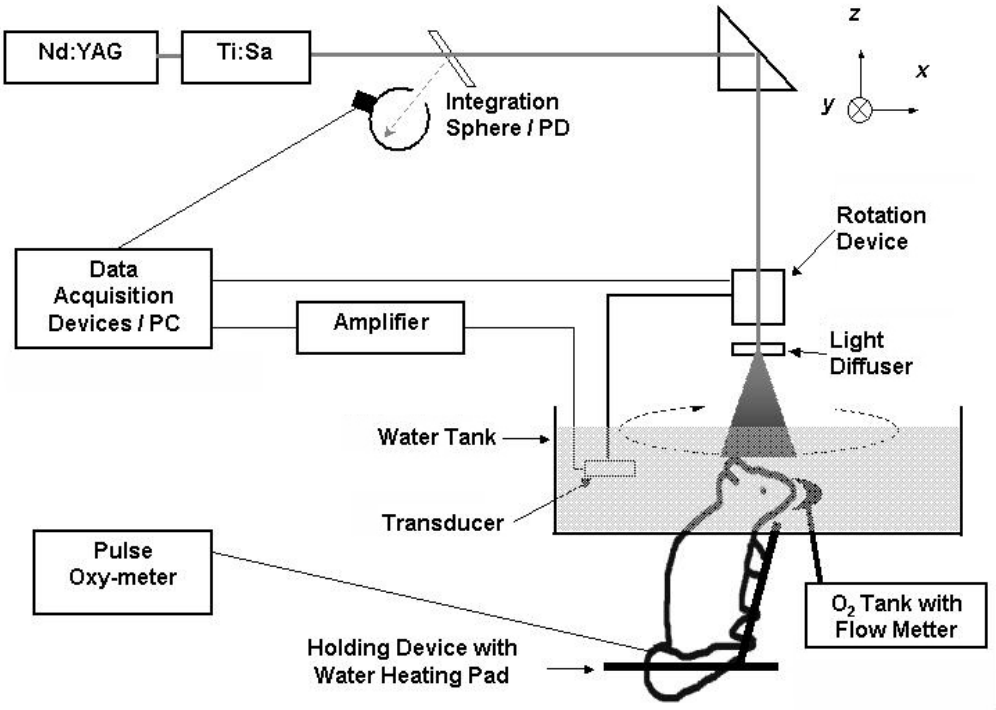

Figure 4. Experimental setup of *in vivo* spectroscopic photoacoustic tomography for small animal.

Cell culture and animal protocols

All the performed experimental animal procedures on the nude mice were approved by the University Laboratory Animal Care Committee of Texas A&M University and followed the guidelines of the Guide for the Care and Use of Laboratory Animals prepared by the United States National Institutes of Health.

U87 glioblastoma tumour cells were used for implantation into young adult immunocompromised nude mice (Harlan, Co.). The cell line is maintained in Dulbecco's Modified Eagle Medium (DMEM) with 10000 Units/ml Penicillin and 10% Fetal Bovine Serum (Gibco, Inc.).

The young adult nude mice weighing about 20 grams were purchased from Harlan, Co., IN and used throughout the study. Stereotactic implantation of graft cells, U87 glioblastoma tumour cells was performed under full anaesthesia using a mixture of ketamine, 87 mg/kg (Ketaset, Forth Dodge Animal Health) and xylazine, 13 mg/kg (AnaSed, Lloyd Laboratories). The cells ($1x10^6$) were inoculated intracranially into the caudate nucleus at 3mm depth from the surface with a volume of 7 µl by using a 10 µl Hamilton syringe. The nude mouse body temperature was controlled at 37°C using water heating pad. The healthy status, pulse rate and the global arterial blood oxygenation, of the mouse were monitored through the entire experiment using pulse oximeter (Model 8600, Nonin Medical, Inc.) which was clamped on the back paw of the nude mouse. U87 glioblastoma tumor cells were inoculated intracranially at 3mm depth from the surface

of the nude mouse head seven days before the PAT experiment. After the experiments, the mice were sacrificed to obtain brain tissue sections/slides. After the slides were fixed, half of them were stained with Thionine to identify the tumor and the other half were stained with anti-von Willebrand Factor viii antibody to demonstrate the tumor-associated neovascularization.

Results and Discussion

Angiogenesis is very critical in the development of tumors because the blood vessels will bring oxygen and nutrients and remove metabolic wastes. Von Willebrand Factor (Factor VIII Related Antigen - VWF-VIII) is a widely used endothelial cell markers for studying angiogenesis/neovascularization.[23] Fig. 5(a) shows the photography of anti-von Willebrand Factor antibody stained saggital section of the mouse brain implanted with U87 glioblastoma tumor. Fig. 5(b) and (c) are the microscope images (40x mag.) of the normal and tumor areas of the brain section which are indicated by characters “b” and “c” in Fig. 5(a) respectively. It is clearly that the tumor tissue contains more irregularly oriented blood vessels than normal tissue.

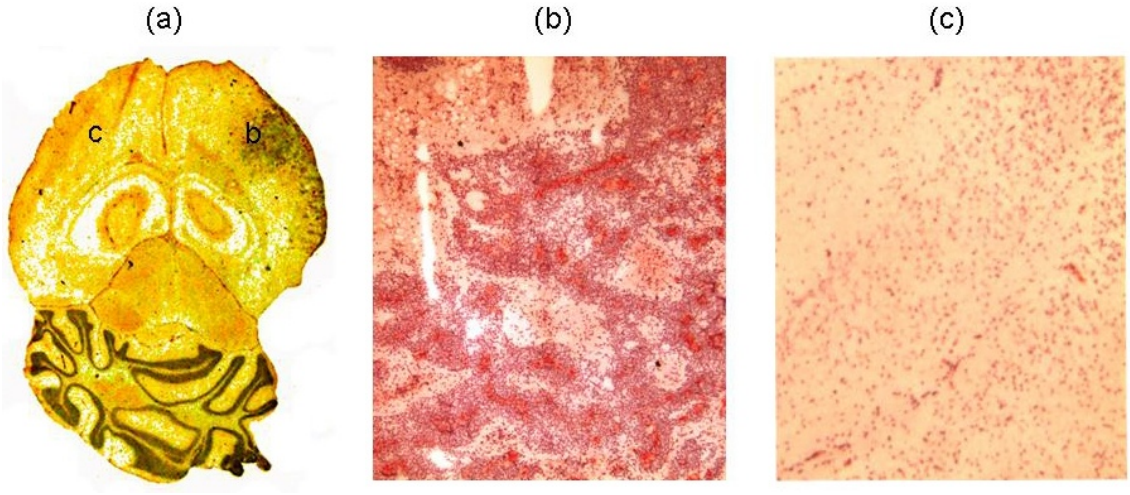

Figure 5. Mouse brain section images.

(a) Photography of anti-von Willebrand Factor viii antibody stained saggital section of the mouse brain implanted with U87 glioblastoma tumor; (b) microscope image (10x mag.) of tumor area in (a) which is indicated by letter b; (c) microscope image (10x mag.) of normal brain area in (a) which is marked by letter c.

To enhance contrast in the normally colorless tissue sections, some tissue sections are stained with Thionine which will stain the cell nuclei. Compared to the normal brain tissue the brain bearing tumors have more compact basophylic hypercellularity with an irregular shape as the circled area shown in Fig. 6(b). Figs. 6(a) and (b) show the tumor located at the right side in the brain. Tumor hypoxia was imaged by the spectroscopic PAT, as shown in Fig. 6(d). The cortex vessels in Fig. 6(a) can be matched with Fig. 6(c) the brain total hemoglobin concentration image. Fig. 6(d) is obtained by masking the blood oxygen saturation image with brain total hemoglobin concentration image. Fig. 6(c) and (d) are acquired seven days after the U87 glioblastoma tumor cells inoculated.

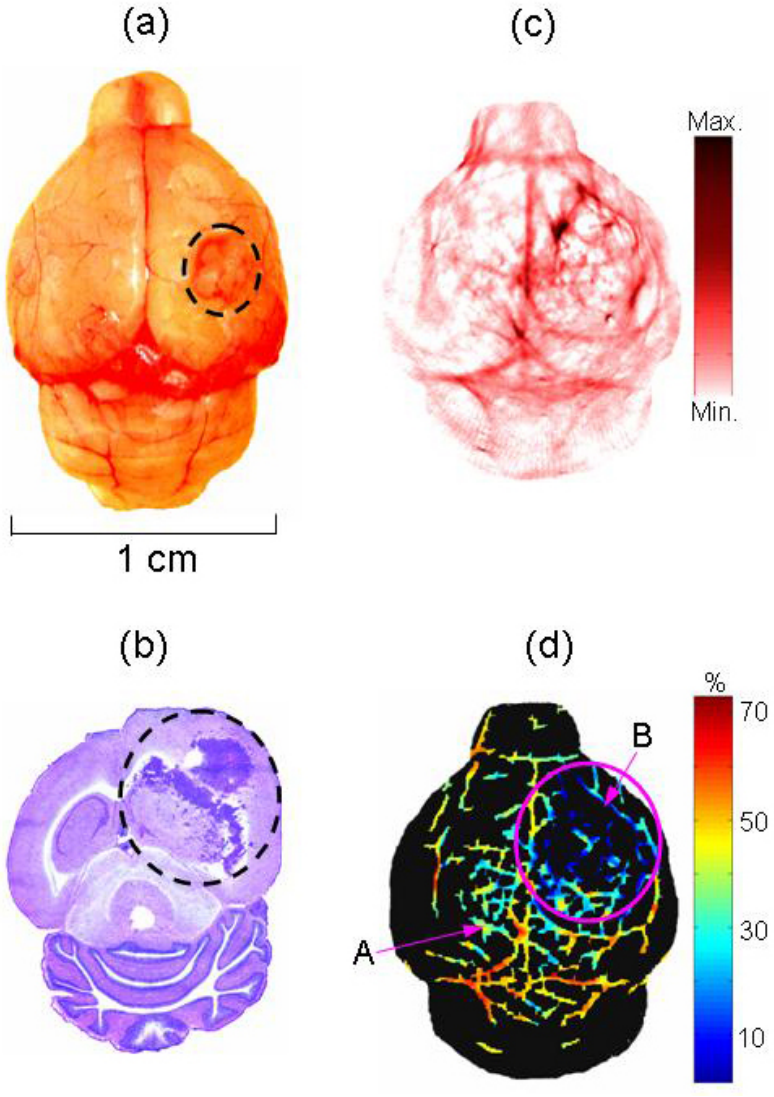

Figure 6. PAT and histology images. (a) Photography of a nude mouse brain inoculated with U87 glioblastoma tumor; (b) Thionine-stained frozen, saggital section of the mouse brain implanted with U87 glioblastoma tumor; (c) the brain total hemoglobin concentration image; (d) estimated brain blood oxygen saturation image; (c) and (d) are simultaneously obtained from noninvasive in vivo spectroscopic PAT; the circles indicate the tumour location, right caudate nucleus and cortex.

Hypoxia occurred at the circled tumor area in Fig. 6(d) due to structural and functional abnormalities of the tumor microvasculature, increased diffusion distances, and tumor-associated anemia.

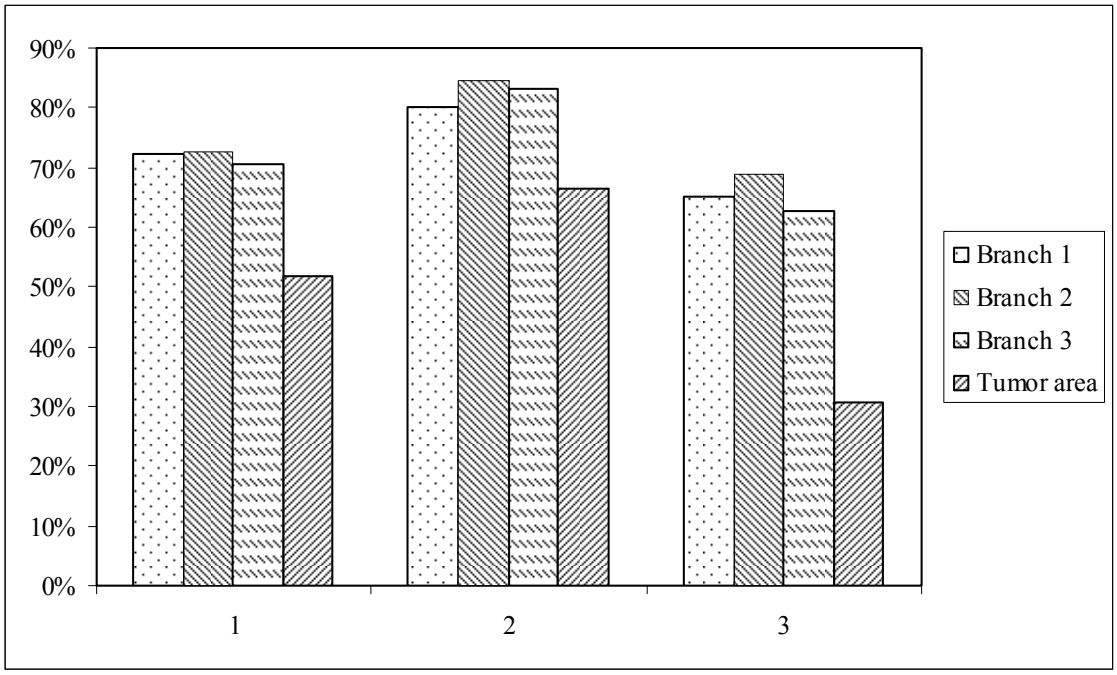

Figure 7. Average SO2 values of 4 blood vessels obtained by spectroscopic PAT from 3 mice. Y axis values of branch 1, 2 and 3 bars are the mean values of SO_2 in branch blood vessels located on the cortex surface of the nude mice which have same topology positions as the blood vessel indicated by arrow "A" in Fig. 3(d). The y axis value of 4^{th} bars in 3 groups is the mean value of SO_2 in blood vessels which have same topology positions as the blood vessel indicated by arrow "B" in Fig. 3(d).

Conclusion

Noninvasive functional imaging and quantification of brain tumor hemoglobin concentration and hemoglobin oxygenation through the intact skin and skull with satisfactory spatial resolution is a difficult task, yet it is very important parameter in underpinning the pathophisiology of tumor development.

There are 3 groups of bars in Fig. 7, each group represents the spectroscopic PAT experiment data acquired from one nude mouse. Y axis values of branch 1, 2 and 3 bars are the mean values of SO_2 in branch blood vessels located on the cortex surface of the nude mice which have same topology positions as the blood vessel indicated by arrow "A" in Fig. 6(d). The y axis value of 4^{th} bars in 3 groups is the mean value of SO_2 in blood vessels which have same topology positions as the blood vessel indicated by arrow "B" in Fig. 6(d). Obviously the tumor tissue is hypoxia since the SO_2 value at tumor tissue is lower than the normal brain tissue. From Fig. 7 and Fig. 6, we can conclude that spectroscopic PAT can assess point-by-point functional parameters and changes in tumor areas in the brain quantitatively with high spatial resolution which will provide better understanding of tumor biology and potential use to new approaches for tumor therapy.

The absorption, scattering and refractive index of the nude mouse head tissues as functions of wavelength which will affect the distribution of optical energy in the head

need to be studied in more detail. Spectroscopic PAT three-dimensional functional brain imaging should be implemented to improve the depth resolution which will increase the accuracy of the measurement. An ultrasonic transducer array should be used to reduce the imaging time and make real-time imaging become feasible.

CHAPTER IV

SIMULTANEOUS TUMOR A_VB_3 INTEGRIN AND OXYGENATION MEASUREMENT

Overview

Here we present simultaneous noninvasive *in vivo* molecular imaging and tumor oxygenation imaging using spectroscopic photoacoustic tomography (PAT), which detects absorption spectroscopic differences among molecular targeting contrast agent, oxyhemoglobin (O_2Hb), and deoxyhemoglobin (HHb). Nude mice brains with intracranially implanted glioma tumors were imaged by SPAT after a tumor targeted contrast agent was systematic administrated through tail vein. We successfully obtained image of the contrast agent distribution around tumor inside mouse brain with high spatial resolution, which has been impossible using conventional optical molecular imaging modalities because of light scattering. In addition to molecular contrast, SPAT visularized the brain oxygenation images in which tumor hypoxia clearly seen. This new imaging method can be useful for visualization of various molecular targeting agents and its delivery for drug development along with metabolic activities around tumours for therapeutic purpose.

Introduction

Molecular imaging is the characterization and measurement of biological processes in living animals at the cellular and molecular level. The study of molecular imaging will lead to better methods for studying complex disease pathways, diagnosing disease at the earliest causative stages.

Spectral PAT is a mixed noninvasive imaging modality that takes advantage of both high optical contrast and high ultrasound resolution without ionizating radiation.[24] Short pulse electromagnetic wave in the visible or NIR region irradiates the imaging object to generate photoacoustic waves according to the thermoelastic mechanism. The distribution of electromagnetic absorption can be reconstructed using the detected photoacoustic signals. The absorption spectrum for each reconstructed image element was found by changing wavelength of radiation source, and the spatial distribution of molecular agent can be extracted by analysing it. Compare to other molecular imaging systems, spectral PAT has the ability to image not just the molecular contrast agents distribution but also other major absorbers in the simultaneously with high spatial resolution (~60 μm)[25] and satisfactory penetration depth (~ 5cm)[26]. In the NIR spectral region, these three absorbers inside small animal dominate the photoacoustic signal. They are the dominant absorbers in the mouse brain in the NIR spectral region under study. Within NIR range, the penetration depth of light in this range is greater than the size of the imaged brain vessel branches (<50 μm) within intracranial tumor. Cerebral

blood oxygenation changes are crucial to understanding the mechanism of functional cerebral metabolism and pathophysiology. Tumor hypoxia is very important in tumor biology and therapy. Hypoxia stimulates tumor cells' production of acids; the hypoxia and acidity of tumors have important consequences for anti-tumor therapy and can contribute to the progression of tumors to a more aggressive metastatic phenotype.[27, 28, 29] SPAT measurements at three wavelengths are sufficient for an absolute estimation of the molecular contrast agent distribution, HbT and SO_2 since they are the dominant absorbers in the mouse brain in the NIR spectral region under study. Within NIR range, the penetration depth of light in this range is greater than the size of the imaged brain vessel branches (<50 μm).

Material and Methods

Cell culture and animal protocols

All the performed experimental animal procedures on the nude mice were approved by the University Laboratory Animal Care Committee of Texas A&M University and followed the guidelines of the Guide for the Care and Use of Laboratory Animals prepared by the United States National Institutes of Health.

U87 glioblastoma tumour cells were used for implantation into young adult immunocompromised nude mice (Harlan, Co.). The cell line is maintained in Dulbecco's Modified Eagle Medium (DMEM) with 10000 Units/ml Penicillin and 10% Fetal Bovine

Serum (Gibco, Inc.). Stereotactic implantation of the U87 glioblastoma tumour cells was performed on the nude mice weighing about 20 grams under full anaesthesia using a mixture of ketamine, 87 mg/kg (Ketaset, Forth Dodge Animal Health) and xylazine, 13 mg/kg (AnaSed, Lloyd Laboratories). The cells ($1x10^6$) were inoculated intracranially into the caudate nucleus at 3mm depth from the mouse head surface with a volume of 7 µl by using a 10 µl Hamilton syringe.

The molecular contrast agent was injected through mouse tail vein with a dosage of 20 nM per rat. The experiment is conducted 20 hours after the contrast agent administration. The nude mouse body temperature was controlled at 37°C using water heating pad. The healthy status, pulse rate and the global arterial blood oxygenation, of the mouse were monitored through the entire spectroscopic photoacoustic experiment using pulse oximeter (Model 8600, Nonin Medical, Inc.) with a detector clamped on the back paw of the nude mouse. After the experiments, the mice were sacrificed to obtain brain tissue sections/slides. One third of the slides were imaged using Odyssey fluorescence microscanner at 800 nm to verify the WW307 uptake. After the other two thirds of slides were fixed, half of them were stained with Thionine to identify the tumor, the other half were stained with anti-von Willebrand Factor viii antibody to demonstrate the tumor-associated neovascularization.

Spectroscopic photoacoustic experiments setup

The experimental setup for the *in vivo* spectroscopic photoacoustic tomography of a

nude mouse head is similar to the one shown in Fig. 4. A tuneable Ti:Sa nanosecond pulse laser (LT–2211A, Lotis T II, Minsk, Belarus) pumped by an Nd:YAG laser (LS–2137/2, Lotis T II, Minsk, Belarus) was employed to provide laser pulses with a pulse repetition rate of 10 Hz. The laser beam was expanded by a concave lens and homogenized by a light diffuser and then was delivered to the animal head. The incident energy density of the laser beam on the surface of the mouse head was controlled at ~ 20mJ/cm^2 (within the ANSI standard). Each single laser pulse's energy was monitored using photodiode (PD) and recorded for normalizing the photoacoustic signal. Two types of ultrasonic transducers (V323/2.25MHz, XMS-310/10MHz, Panametrics) were used as the detectors to receive the induced acoustic signals. The diameters of the active areas are 6 mm for the 2.25 MHz transducers, 2 mm for the 10 MHz transducer. These commercial transducers have nominal bandwidths of 50% to 80% of their central frequencies. A computer controlled step motor drove the 10MHz and 2.25MHz transducers to circularly scan the nude mouse cortical surface and 3mm below respectively the cortical with a radius of 3.5 cm and a step size of 3 degree. Instead of three different wavelengths, four different wavelengths (764nm, 784nm, 804nm and 824nm) were used to increase the measurement accuracy. Photoacoustic signals induced by those four wavelengths were obtained in each scanning step to reduce the motion and contrast agent bleaching artefacts. The nude mouse was fixed by a homemade restrain mount with its head protruding into the water tank through a hole in the bottom of the water tank. The hole was sealed with a piece of polyethylene membrane. The mouse head surface was covered with a thin layer of ultrasonic coupling gel. The detected

photoacoustic signals were amplified and then digitized by an oscilloscope. The digitized signals are transferred to a computer, and the distribution of the molecular contrast agent and the SO_2 in the imaging plane (x-y plane) is calculated and reconstructed after a single full view scanning.

Spectroscopic PAT of molecular and SO_2 imaging

A spectroscopic PAT consists of a calculation of the intensity of the acoustic signal detected by a piezoelectric detector against the excitation wavelength. The wavelength of the excitation laser pulse is varied altering the characteristics of the thermoelastic wave due to the wavelength dependent change in the optical properties of the chromospheres in the tissue. By analyzing the spectrum, we can investigate important properties of varies absorbers in the object, such as concentration, volume, etc.

20 hours after the molecular contrast agent intravenously administrated into the nude mice through the tail vein, there are only three main absorbers (the contrast agent, HHb and O_2Hb) in the NIR range. Then the tissue absorption coefficient at wavelength λ_i can be calculated as

$$\mu_a(\lambda_i) = \varepsilon_{\mathrm{HHb}}(\lambda_i)[\mathrm{HHb}] + \varepsilon_{\mathrm{O_2Hb}}(\lambda_i)[\mathrm{O_2Hb}] + \varepsilon_{\mathrm{ContrastAgent}}(\lambda_i)[ContrastAgent]$$

where $\varepsilon_{\mathrm{HHb}}(\lambda_i)$, $\varepsilon_{\mathrm{O_2Hb}}(\lambda_i)$ and $\varepsilon_{\mathrm{ContrastAgent}}(\lambda_i)$ are the known molar extinction coefficients of HHb, O_2Hb and the contrast agent at wavelength λ_i, respectively;[30] $[\mathrm{HHb}]$, $[\mathrm{O_2Hb}]$ and $[ContrastAgent]$ are the molar concentrations of hemoglobin, oxy-hemoglobin and the molecular contrast agent, respectively. The acquired localized PA signal $\phi(\lambda_i)$ is linearly related to the voxel's absorption coefficient after being normalized by the

tissue's optical wavelength-dependent attenuation and the incident light energy, the $\mu_a(\lambda_i)$ in the above equation can be replaced by $\phi(\lambda_i)$ to calculate $[ContrastAgent]$, $[HHb]$ and $[O_2Hb]$under multiple wavelength measurements. Therefore point-by-point images of the molecular contrast agent, HHb and O_2Hb distributions can be calculated using the PA signals and known molar extinction coefficients. The point-by-point SO_2 image can be calculated as

$$SO_2 = \frac{[O_2Hb]}{[O_2Hb]+[HHb]}$$

Results and Discussion

The molecular contrast agent we used for the SPAT non-invasive *in vivo* visualization of U87 tumors with $\alpha_v\beta_3$ integrin expression is an integrin αvβ3-targeted peptide cyclo(Lys-Arg-Gly-Asp-Phe) [c(KRGDf)] labeled with near infrared fluorescence dye IRDye800-NHS (LI-COR, Inc.). c(KRGDf) was synthesized using Fmoc solid phase chemistry on linker-PL-DMA resin. To conjugate the IRDye800-NHS with c(KRGDf), a mixture of IRDye800-NHS (1 eq) and c(KRGDf) (1.3 eq) in dimethylformamide/DIPEA (10/1, v/v) was stirred for 24 hours at room temperature. The compound was purified by reverse-phase HPLC after remove the solvent under vaccum. The product was validated by analytic high-performance liquid chromatography (HPLC) and matrix-assisted laser desorption ionization (MALDI). Molecular SPAT imaging of the contrast agent uptake

by the U87 glioma tumor has the potential to allow early stage cancer detection, unravel the tumor angiogenesis since $\alpha_v\beta_3$'s presence is greatly increased near neo-angiogenesis.

In Fig. 8 (a), the peptide-dye conjugates (red colour) bound specifically to tumor cells (green colour) expressing $\alpha_v\beta_3$. From Fig. 8 (b), premixed with c(KRGDf) blocked the uptake of IRDye800-c(KRGDf) in cell culture because the c(KRGDf) blocked the $\alpha_v\beta_3$ receptor of the U87 cells.

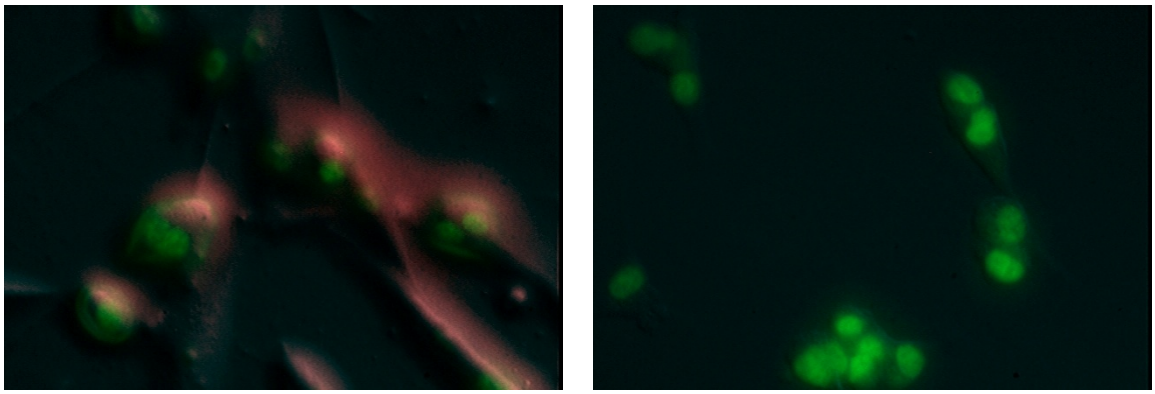

(a) (b)

Figure 8. Fluorescence images of U87 cell culture.

(a) 3 minutes after add 6μM molecular contrast agent in the U87 cell culture; (b) 3 minutes after add 6μM molecular contrast agent in the U87 cell culture which is premix with 1.2μM c(KRGDf) for 5 minutes. Both (a) and (b) are fluorescence microscope images.

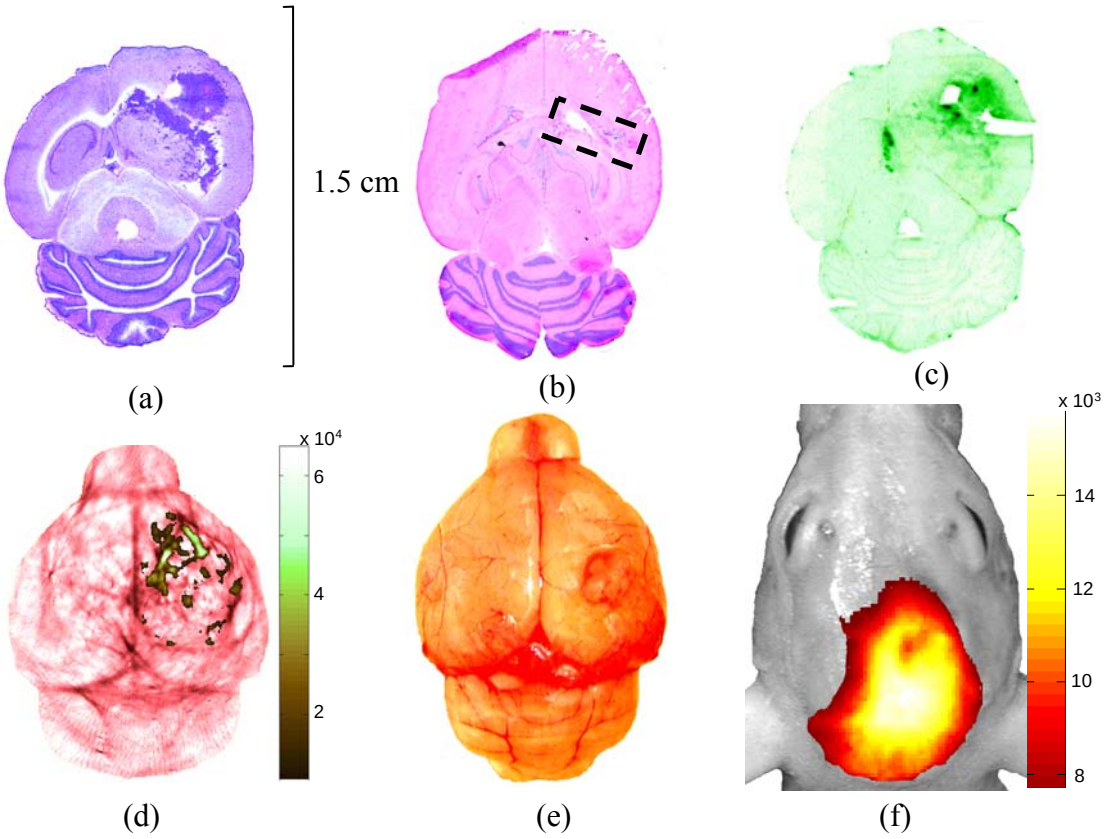

Figure 9. PAT, fluorescence and histology images.

(a) Thionine stained section photo of the nude mouse brain with U87 tumor; (b) Factor-VIII satined section photo; (c) Fluorescence frozen section image of the brain acquired by Odyssey fluorescence microscanner; (d) estimated distribution of the molecular contrast agent in the brain superimposed on the photoacoustic brain structure image; (e) Photography of a nude mouse brain with U87 glioblastoma tumor; (f) fluorescence image of the nude mouse head superimposed on the planar image; estimated brain blood oxygen saturation image. (d) is acquired by noninvasive *in vivo* spectroscopic PAT; (a), (b) and (c) are at the depth of ~1 mm from the brain cortex; the doted areas indicate the tumor positions.

In vivo fluorescent image (Fig. 9 (f)) was acquired on the same nude mouse before the SPAT experiments to verify the molecular contrast agent uptake and compare with the molecular SPAT images.

Fig. 9 (a), (b) and (c) show the tumor located at the right side of the brain. Integrin $\alpha_v\beta_3$–targeted peptide–ICG conjugated NIR fluorescent contrast agent is injected intravenously through the nude mice tail 24 hours before the spectroscopic PAT imaging. The contrast agent is bonded with $\alpha_v\beta_3$ integrin which is over-expressed by newly formed tumor microvessels. The fluorescence images in Fig. 9 (c) and (f) indicate uptaking of the contrast agent in the tumor area. Fig. 9 (d) shows the contrast agent distribution in the brain; it is clearly that the contrast agent is mainly accumulated at the tumor area. Since PAT overcomes the resolution disadvantage of optical imaging caused by the overwhelming light scattering in biological tissue, the resolution of PAT image (d) is higher than the planar fluorescence image (f). Hence, the tumor is more localized in Fig. 9 (d). In addition, tumor hypoxia, which is an important parameter in tumor therapy, was also imaged by the molecular spectroscopic PAT, as shown in Fig. 10 (a).

There are 3 groups of bars in Fig. 10 (b), each group represents the spectroscopic PAT experiment data acquired from one nude mouse. Y axis values of branch 1, 2 and 3 bars are the mean values of SO_2 in branch blood vessels located on the cortex surface of the nude mice which have same topology positions as the blood vessel indicated by arrow "A" in Fig. 9(d). The y axis value of 4^{th} bars in 3 groups is the mean value of SO_2 in

blood vessels which have same topology positions as the blood vessel indicated by arrow "B" in Fig. 9(d). Obviously the tumor tissue is hypoxia since the SO_2 value at tumor tissue is lower than the normal brain tissue. From Fig. 10 and Fig. 9, we can conclude that spectroscopic PAT can assess point-by-point functional parameters and changes in tumor areas in the brain quantitatively with high spatial resolution which will provide better understanding of tumor biology and potential use to new approaches for tumor therapy.

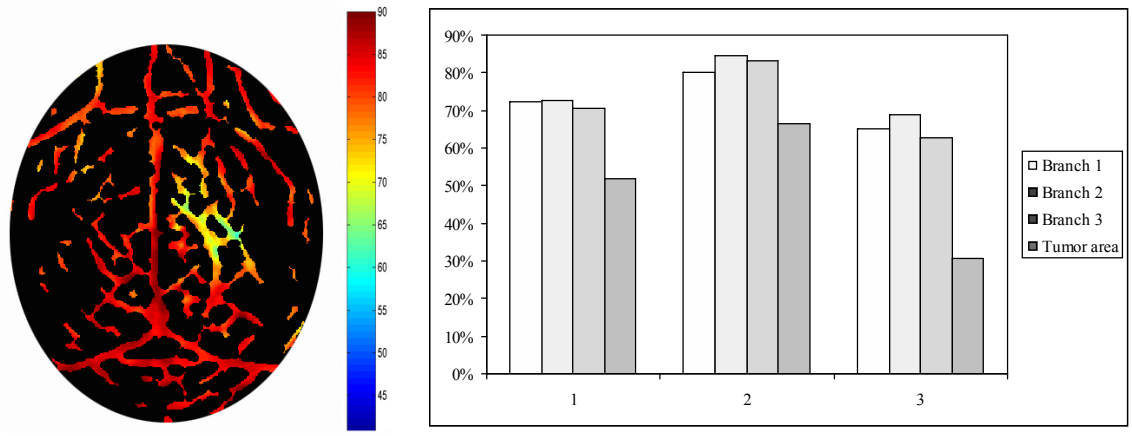

Figure 10. Brain tumor oxygen distribution.

(a) Oxygen saturation image of nude mice brain with U87 tumor; (b) statistical data of SO_2 in cerebral branch blood vessels and tumor area.

Conclusion

During the SPAT experiments, we observed that the maximum molecular contrast agent uptake occurred 20 hours after the tail vein administration using *in vivo* fluorescence imaging. The contrast between the tumor tissue and normal tissue is 2:1.

In order to reduce photobleaching, we used shutter to shorten the laser shining time on the nude mouse head. We found that even there was photobleaching but the absorption bleaching is so small that it can be neglected. Since the SPAT is based on the tissue absorption property, the photobleaching effect of the contrast agent has not affect the accuracy of the uptake measurement.

We can use more wavelengths and consider more compensation factors to increase the accuracy of the contrast agent and SO_2 quantification. There is one drawback in the current SPAT experimental setup. Real time imaging is not possible since it takes 15 minutes to obtain one image under single wavelength. Transducer array system should be used to achieve fast imaging. This new technology can potentially allow the real time detection of cancer in a minimally invasive manner. It could provide immediate diagnostic and therapeutic information to the doctors to assist them on treatment plans even surgeries. This technology can help reduce morbidity and mortality as well as increase survival.

CHAPTER V

TUMOR GLUCOSE METABOLISM

Overview

Glucose uptake in malignant glioblastoma tumor can be used to estimate the overall metabolic activity since glucose is the primary energy source. It is a very useful indicator for cancer detection, therapy design and treatment monitoring. In this study, fluorescent 2-deoxyglucose analog, 2-[N-(7-nitrobenz-2-oxa-1,3-diaxol-4-yl)amino]-2-deoxyglucose, was used for assessing glucose uptake in U87 glioblastoma cell culture and U87 xenograft mice tumors. Multiphoton microscopy images showed that U87 cells uptake the glucose analog quickly in the first 8 minutes and then a relatively steady concentration is reched. With the presence of D-glucose, the glucose analog uptake was significantly decreased. In the retention study, the glucose analog was decayed rapidly in the first 10 minutes then slowly degrading and the fluorescence signals remain a certain level after 48 minutes. The in vivo fluorescence images of nude mice with U87 xenograft subcutaneous tumor displayed a maximum uptake at 15 hours after the glucose analog was injected intravenously through the tail vein. Due to the malignant glioblastoma tumor high glucose metabolic rate, the tumor tissue showed very high fluorescence signals compare to the surrounding normal tissue. At 15 hours post

injection, glucose was cleared from blood stream, heart, spleen and lung as showed in the clearance experiment results.

Introduction

Almost all of the foods we take every day are carbohydrates. The enzymes in the mouth and small intestine help to breakdown carbohydrates to make glucose and then absorbed into the blood stream. The pancreas insulin regulates the glucose levels in the blood stream by unlock/lock the cell's glucose channels. Insulin molecules bind to their associated receptors and promote the uptake of glucose into various tissues that contain glucose transporters. Glucose is completely broken down during cellular respiration and 38 ATP molecules are formed as the primary energy source for cellular work[31]. Based on the existence of a high consumption of glucose and high glycolysis by most tumor cells due to an increase in metabolic activity, glucose uptake monitoring can be used for cancer detection, therapy development and treatment effectiveness validation .[32,33]

2-[N-(7-nitrobenz-2-oxa-1,3,diazol-4-yl)amino]-2-deoxyglucose (2-NBDG) is a fluorescence glucose analog developed by Yoshioka K., et al.[34]. This fluorescently labeled glucose probe can be used as an excellent glucose uptake marker for normal nonmalignant cells (bacteria, yeast and mammalian cells) and malignant tumor cells. 2-NBDG uptake rate has been proved similar to 2-Deoxyglucose (2-DG). Hexokinase enzyme phosphorylates the 2-NBDG at the C-6 position after the uptake, thus the

glucose analog will be trapped inside the cell[35,36]. NBD fluorophore group in the 2-NBDG is sensitive to environment but usually displays intense fluorescence with excitation/emission maxima of 465nm/540nm. Previous studies showed that 2-NBDG and D-glucose are competing for the glucose transporter to enter the cell which implies that 2-NBDG is using same transportation mechanism as glucose[37].

Conventional fluorescence tomography was used for *in vivo* U87 xenograft nude mice tumor glucose uptake study using 2-NBDG glucose analog. Fluorescence is an efficient light-emitting process that is triggered by the absorption of the excitation radiation of an appropriate wavelength. The fluorescence signal emitted by a molecule or atom after optical excitation is easily detected even at very low concentrations. Light energy is 'packaged' into discreet bundles called photons. After fluorophores absorb light of certain wavelengths, their electrons transform into an unstable exited state then rapidly lose excess energy and emit light. Proper optical filters can be used to distinguish the excitation and emission lights since the energy of the emitted light is smaller than the absorbed light which means longer wavelength and different color.

In this research, multiphoton excitation microscopy was implemented for monitoring U87 glioblastoma tumor cells 2-NBDG uptake and retention. The laser source is sub-10-Femtosecond pulses and has spectra centered at 800 nm with a full width at half-maximum (FWHM) of 133 nm. The NBD fluorescent dye is excited at twice the wavelength used in ordinary fluorescence observations by absorbing the energy of two

photons simultaneously. Since the photon energy is inversely proportional to the wavelength, the multiphoton microscopy excitation photon energy is much lower than conventional fluorescence imaging. Because the excitation probability of the fluorescent dye in multiphoton excitation is proportional to the square of excitation light intensity, only the area proximal to the focal point, where the photon density is high, can be excited. Due to the above two reasons, fading of fluorescent dye and damage to tumor cells from the excitation light are reduced and limited locally. High 1 micrometer resolution is achieved by combining multiphoton excitation with the confocal technique in the multiphoton imaging device used for this study[38,39].

Material and Methods

Cell culture and animal protocol

All the performed experimental procedures on the U87 tumor cells and nude mice were approved by the University Laboratory Animal Care Committee of Texas A&M University and followed the guidelines of the Guide for the Care and Use of Laboratory Animals prepared by the United States National Institutes of Health.

U87 glioblastoma tumour cells were used for multiphoton imaging *in vitro* experiment. The cell line was maintained in Dulbecco's Modified Eagle Medium (DMEM) with 10000 Units/ml Penicillin and 10% Fetal Bovine Serum (Gibco, Inc.). Subcutaneous implantation of the U87 tumour cells was performed on the nude mice weighing about

20 grams under full anaesthesia using a mixture of ketamine, 87 mg/kg (Ketaset, Forth Dodge Animal Health) and xylazine, 13 mg/kg (AnaSed, Lloyd Laboratories). The cells ($1x10^6$) were inoculated subcutaneously above the medal of skull with a volume of 7 µl by using a 10 µl Hamilton syringe. The mice were anaesthetized again for noninvasive *in vivo* fluorescence imaging when the tumor's diameter reached 5 mm. For the multiphoton microscopy experiments, monolayer of U87 cells was attached to the inner bottom of a petri dish (35x10 mm) for imaging. A modified balanced salt solution (MBSS) was used for washing away nonuptake 2-NBDG from the cells.

The 2-NBDG glucose analog was injected through mouse tail vein with a dosage of 0.1 mg per mouse when the diameter of the tumor reached 5 mm. The *in vivo* fluorescence imaging experiment was conducted 15 hours after the contrast agent administration. The nude mouse body temperature was controlled at 37°C using water heating pad. After the experiments, the mice were sacrificed to obtain various organs' fluorescence images to verify the glucose uptake and clearance.

Multiphoton microscopy

The light source for the multiphoton microscopy is sub-10-fs pulses from a Kerr-lens mode-locked $Ti:Al_2O_3$ oscillator (Femtosource Compact, Femtolasers) pumped by a frequency-doubles $Nd:YVO_4$ solid-state laser (Verdi, Coherent). The laser light is coupled into the epifluorescence port of an upright microscope (Axioskop2 MAT, Zeiss) via dual-axis galvanometer driven mirrors (Cambridge Technology) mounted on an

elevated breadboard and controlled by a three-axis control board (Vista, ISS). The beam is directed to the microscope objective by a short-pass dichroic mirror (635dcspxruv3p, Chroma). Nonlinear optical signals are collected by the focusing objective and directed to detector unit mounted on an accessory port of the binocular head. Image intensity signals are collected and displayed in counts per second on a PC and analyzed by Matlab (The MathWorks, Inc., Natick, MA) and Photoshop (Adobe Systems, Inc., San Jose, CA).

Fluorescence tomography

The non invasive *in vivo* fluorescence imaging setup is similar with the one in figure 2 for nude mice with 2-NBDG glucose analog contrast agent. The mouse was illuminated with light from halogen lamp in a dark chamber filtered by BG25 glass with a 400 nm center wavelength. A macro lens, coupled with cooled CCD camera, collected the emitted fluorescent light from the 2-NBDG molecules. The lens was fitted with a bandpass filter with 540 nm center wavelength. Images were acquired and stored using the application that came with the CCD camera. Matlab (The MathWorks, Inc., Natick, MA) and Photoshop (Adobe Systems, Inc., San Jose, CA) were used to process and analyze the images.

Results and Discussion

Multiphoton microscopy study

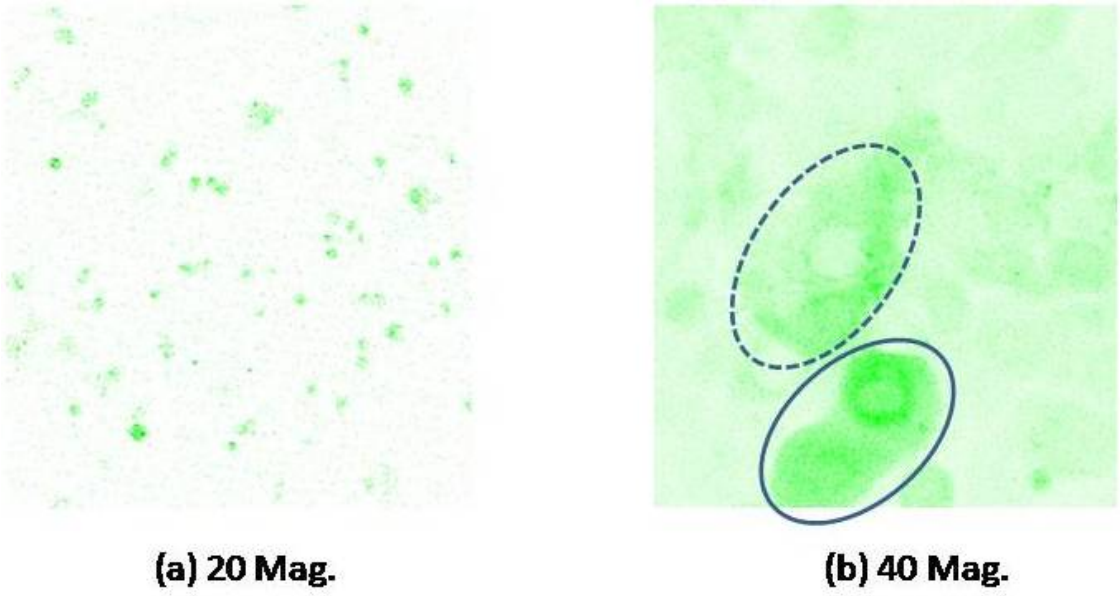

Figure 11. Multiphoton images of U87 cell culture.

Multiphoton microscopy images of U87 tumor cells obtained 10 minutes after adding 0.1 mM 2-NBDG glucose analog (a. 20 Mag.; b. 40 Mag).

10 minutes after 0.1 mM 2-NBDG was added to the petri dish with a monolayer of U87 cells attached on the inner bottom, the cells were washed in MBSS and multiphoton microscopy images were collected (Fig. 11.). In Fig. 11 (b), the glucose analog went through the dash circled cell's membrane and distributed in the cytoplasm but not in the cell nucleus. The lower solid line circled cells are in the telophase of mitosis. In this phase, the cell's dividing requires high glucose metabolism rate to produce enough

energy especially in perinuclear area due to the graduate reformation of nuclear envelope. This is consistent with the multiphoton microscopy image, the glucose analog went through the nuclear envelope and the perinuclear area has more condensed 2-NBDG signals.

Because the high nanometer resolution and high sensitivity, the multiphoton microscopy could be used to detect and monitor molecular level changes. Noninvasive *in vivo* imaging of glucose metabolism is difficult because the optical characteristics of glucose. The fluorescence glucose analog 2-NBDG was used as a contrast agent for imaging glucose metabolism successfully in this study. By combining the merit of multiphoton microscopy and fluorescence glucose analog, high resolution imaging of cell glucose activities can be achieved.

The time dependent U87 cells 2-NBDG uptake is shown in Fig. 12. line (a). Three minutes after the U87 cells immersed in 0.1 mM 2-NBDG with MBSS, a series of multiphoton microscopy images were taken at 10 seconds per frame for 30 minutes. Same as Fig. 12 line (c) and (e), each data point on line (a) is the average fluorescence signal strength calculated from one multiphoton microscopy image contains about 30 cells at the specific time point. The data line (a) was made from more than 200 images (images are not shown). The lines (b), (d) and (f) are trend lines for the corresponding data lines. According to the fluorescence signal strength recorded, the maximum uptake

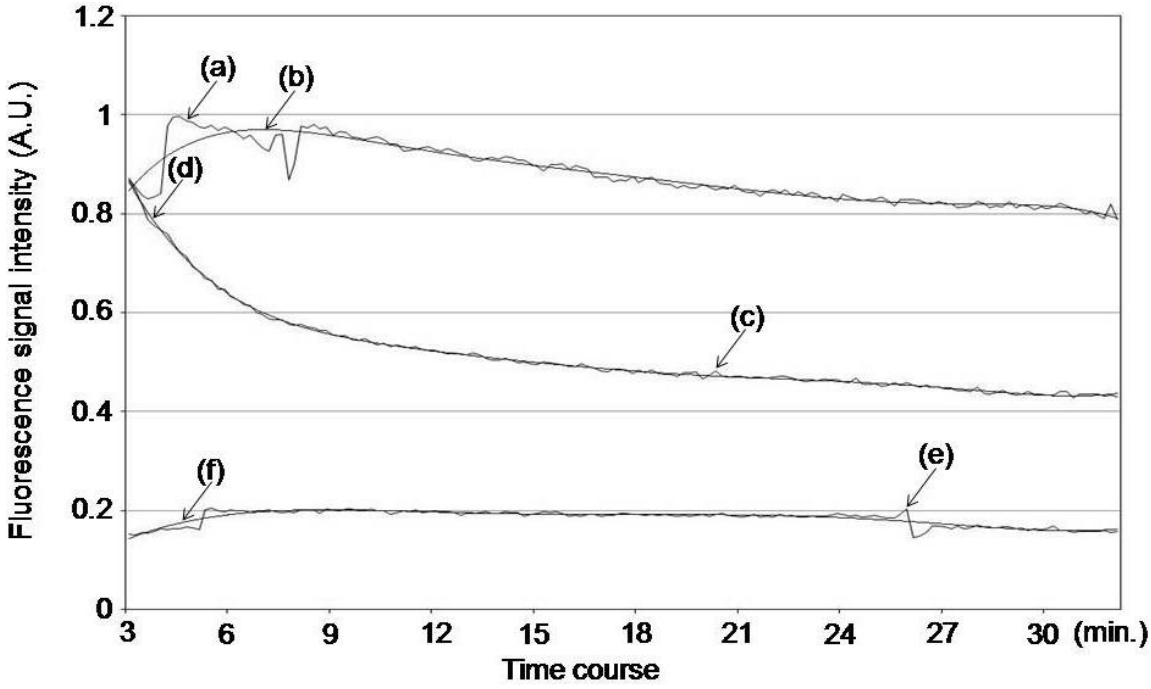

Figure 12. U87 tumor cells glucose metabolism study.

Using 2-NBDG measured by multiphoton microscopy. X axis is the time course in minutes and the Y axis shows the fluorescence signal strength in arbitrary unit. (a) Changes of fluorescence signal strength within 37 min. after adding 0.1 mM 2-NBDG; (b) trend line for (a); (c) Retention of fluorescence signal strength within 48 min. after incubation for 20 min. with 0.1 mM 2-NBDG; (d) trend line for (c); (e) Changes of fluorescence signal strength after adding 0.1 mM 2-NBDG with the presence of 5 mM D-glucose; (f) trend line for (e).

occurred at 7.5 minutes then the glucose signal was decayed slowly. To assess the glucose retention of U87 cells, the cells in the petri dish were exposed to 0.1 mM 2-NBDG for 20 minutes, then washed with MBSS and fixed on the multiphoton microscope for imaging. The analyzed retention data was shown in Fig. 3. line (c). The

fluorescence signals of the glucose analog were decayed quickly during the first 10 minutes then slowly degrade. Fig. 12. Line (e) is the experiment result for glucose analog uptake with the presence of D-Glucose. The U87 cells were exposed to 0.1 mM 2-NBDG and 5 mM D-Glucose at the same time. Compare the line (e) signal strength with line (a) and (c), it showed that the 2-NBDG concentration in the cells is lower due to the competition of D-Glucose. This result verified that the 2-NBDG is a valid glucose analog since it uses same transportation pathway, glucose transporter (GLUT), as glucose.

Based on the data from the above experimental results and the facts that 2-NBDG will be phosphorylated and decompose to a non-fluorescence derivative at the C-6 position in the cell (Yoshioka, 1996), our study confirmed that the U87 tumor cell dynamic glucose metabolism equilibrium can be monitored by the multiphoton microscopy. The glucose was uptaken by the U87 cells quickly (~8 minutes) and then saturated at a relatively stable state. Without glucose supplement, the glucose was consumed by the U87 cells quickly at the first 10 minutes then gradually decomposed overtime.

In vivo fluorescence tomography study

0.1 mg 2-NBDG in 0.1 mL MBSS was injected through the nude mouse tail vein, the noninvasive *in vivo* fluorescence images were taken every 5 hours for 25 hours (Data is not shown). The maximum tumor fluorescence signal strength was detected at 15 hours after the 2-NBDG injection as showed in Fig. 13. after coregistered with white image.

The tumor region on the mouse head has significantly strong fluorescence signal intensity compare to the background due to the fact that the malignant U87 tumor has high glucose metabolism which consistent with the characteristic of malignant tumors.

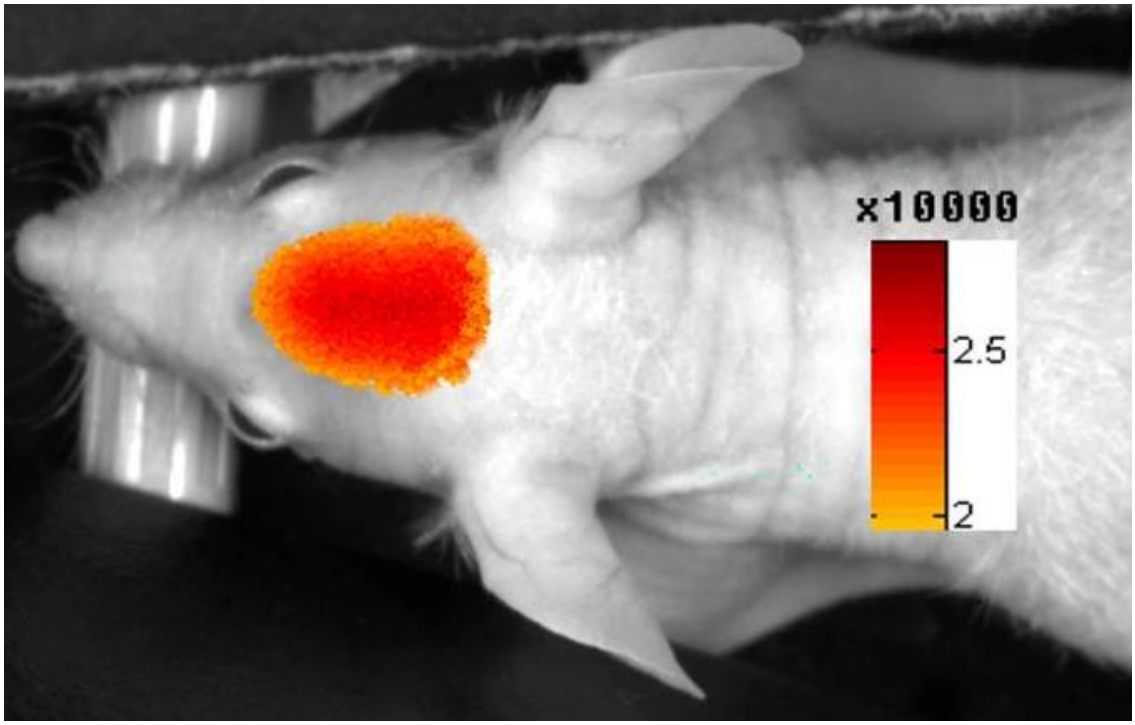

Figure 13. Nude mouse with U87 subcutaneous tumor noninvasive *in vivo* fluorescence image. Coregistered with white image obtained 15 hours after 0.1 mg 2-NBDG tail vein injection.

Another set of control nude mice were sacrificed 15 hours after the 2-NBDG administration for 2-NBDG clearance study. The fluorescence images of various tissue/organ were taken as showed in Fig. 14. The tumors have strong fluorescence signal compare to other organs such as intestines, kidney and liver. The heart, blood,

spleen and lung did not have any fluorescence signals which implied that the glucose analog already has been cleared out from these blood stream and organs.

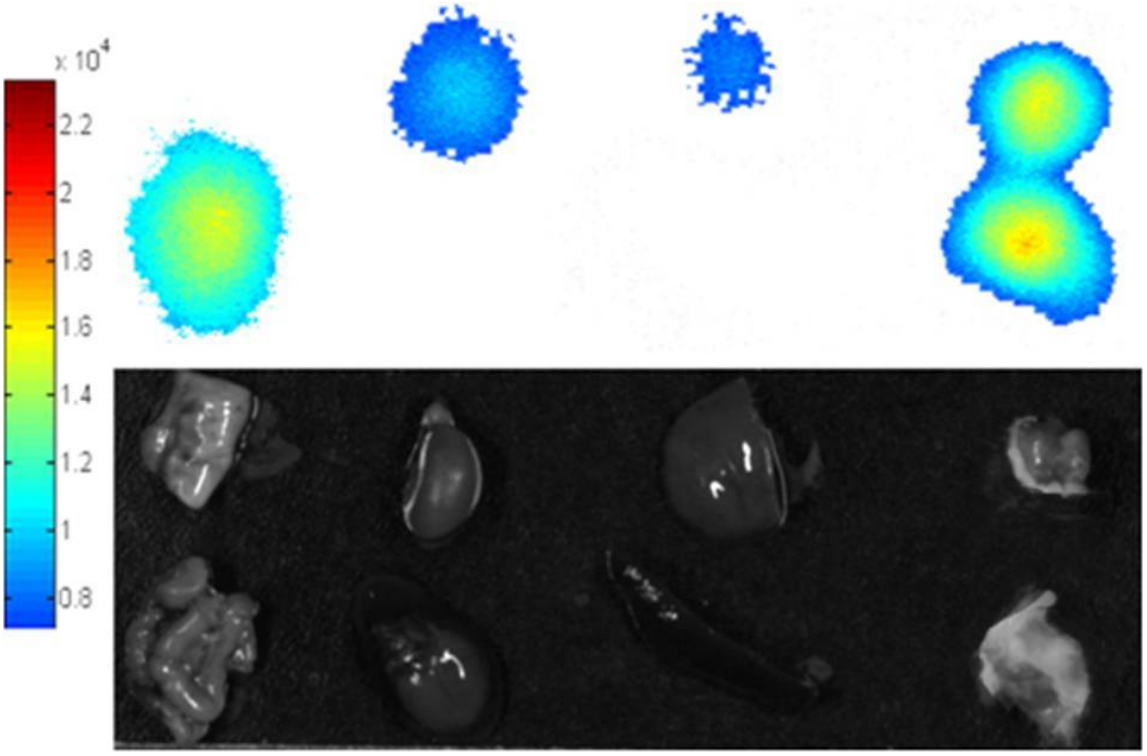

Figure 14. Fluorescence images and white images of dissected nude mouse organs/tissues. (lung, intestine, kidney, heat with blood, liver, spleen, tumors) obtained 15 hours after 2-NBDG tail vein injection.

Conclusion

Our preliminary study showed that by combining multiphoton microscopy and *in vivo* fluorescence imaging using 2-NBDG glucose analog, both the U87 cell activities and

whole tumor glucose metabolism can be successfully studied in cell culture and live animal.

This demonstrates the possibilities to use multiphoton microscopy and fluorescence imaging technique with the assistance of fluorescence glucose analog to study glucose metabolism. In the future, we will study the multiphoton microscopy glucose imaging using multiple wavelengths at the same time with various fluorescence glucose analogs. Noninvasive in vivo nanometer resolution live animal multiphoton imaging will be implemented to study the tumor glucose metabolism in details.

CHAPTER VI

TUMOR CELL AMINO ACID METABOLISM

Overview

The abnormal amino acid metabolism and protein synthesis are very common in cancer patients. Neoplastic cells can irreversibly consume the essential amino acids from the cancer host due to the nature of tumor cell enzymes. The monitoring amino acid metabolism is very important for cancer detection, cancer development monitoring, therapy design and evaluation of the therapy effects. Ion exchange chromatography or specially adapted reverse phase-high performance liquid chromatography (RP-HPLC) to evaluate tumor tissue free amino acid is a popular application for tissue biopsy to study the amino acid and protein metabolism. These methods are time consuming and also cannot be done *in vivo* even in experimental animals. In this study, a novel preliminary method is presented for studying free amino acid, which also has the potential to be used for experimental animals *in vivo*. With the presence of free amino acid targeted Cy 3.5 NHS ester, the free amino acid distributions were showed clearly by acquired multiphoton tomography images in (N-ethyl-N-nitrosourea) ENU (not mammary carcinoma) cell culture and by *in vivo* fluorescence images in live rat bearing ENU tumor xerograph.

Introduction

The fate of amino acids and their metabolism can be conveniently grouped under three paths. First, protein synthesis utilizes amino acids as the basic materials in all tissue. Second, amino acids are precursors for the synthesis of various nitrogenous small molecules. Third, amino acids in excess of requirements degrade and eventually form urea exclusively in the liver[40].

Disorders of amino acid metabolism are among the most common of the inborn errors of human metabolism which are defects that arise from abnormal protein synthesis. The abnormal amino acid metabolism and protein synthesis can also be found in cancer carriers. By virtue of tumor cell enzymes, neoplastic cells can irreversibly drain the host of essential amino acids[41].

The tumor-bearing animals were in negative energy balance but in overall positive nitrogen balance due to the growth of the tumor. The food intake decrease and the body lipids, which provide the energy for the tumor growth, are gradually exhausted and the animals with tumor become cacotrophia. The nitrogen, which was necessary for the proliferation of the tumor, was made available by a net breakdown of skeletal muscles. Muscle protein turnover accounts for a significant proportion of whole body protein turnover. Therefore, any reduction in muscle turnover is a suitable way to save energy and to channel amino acids toward protein synthesis and gluconeogenesis elsewhere[42].

The monitoring amino acid metabolism is very important for cancer detection, cancer develop monitoring, therapy design and evaluation of the therapy effects. For example, folate (One-carbon amino acid) anti-metabolites such as methotrexate were decided to be used in cancer chemotherapy after the study of amino acids metabolism. The tumor has high rate of proliferation, and hence a high requirement for folate for DNA synthesis, but has only very limited reserves. Alternating therapy with folate anti-metabolites, followed by repletion with massive doses of folate, seems to be effective in many cases[43].

In this study, I present a novel preliminary method for fast evaluate amino acid metabolism by studying free amino acid. This method has the potential to be used on experimental animals *in vivo*. Multiphoton excitation microscopy and *in vivo* conventional fluorescence tomography with the presence of Cy3.5 N-hydroxysuccinimide (NHS) ester contrast agent were used in this method.

Multiphoton excitation microscopy is a technique that uses non-linear optical effects to achieve optical sectioning. The sample is illuminated with a wavelength around twice the wavelength of the absorption peak of the fluorophore being used. For example, in the case of fluorescein which has an absorption peak around 500nm, 1000 nm excitation could be used. Essentially no excitation of the fluorophore will occur at this wavelength. However, if a high peak-power, pulsed laser is used (so that the mean power levels are moderate and do not damage the specimen), two-photon events will occur at the point of focus. At this point the photon density is sufficiently high that two

photons can be absorbed by the fluorophore essentially simultaneously. This is equivalent to a single photon with energy equal to the sum of the two that are absorbed. In this way, fluorophore excitation will only occur at the point of focus (where it is needed) thereby eliminating excitation of out-of-focus fluorophore and achieving optical sectioning.

Material and Methods

Cell culture and animal protocol

All the performed experimental procedures on the N-ethyl-N-nitrosourea (ENU) tumor cells and rats were approved by the University Laboratory Animal Care Committee of Texas A&M University and followed the guidelines of the Guide for the Care and Use of Laboratory Animals prepared by the United States National Institutes of Health. Chemicals and solutions were obtained from Sigma Chemical Co.(St. Louis, MO, USA) unless otherwise indicated.

The ENU1564 tumor cell line used in this study was originally developed in our laboratory and originated from an *N*-ethyl-*N* nitrosourea-induced mammary adenocarcinoma in a female Berlin-Druckrey IV (BD-IV) rat. This cell line is highly metastatic to brain and bone tissues (30). Prior to imaging experiments, the cell line was maintained in Dulbecco's modified Eagle's medium (DMEM) (Invitrogen, Carlsbad, CA, USA), supplemented with 10% fetal bovine serum (Invitrogen) and antibiotics (100

units/ml penicillin and 100 µg/ml streptomycin). For the multiphoton microscopy experiments, monolayer of ENU cells was attached to the inner bottom of a petri dish (35x10 mm) for imaging. A modified balanced salt solution (MBSS) was used to wash the cells since DMEM will give strong background fluorescence signals.

Cy3.5 NHS ester (GE Healthcare Bio-Sciences, Piscataway, NJ, USA)

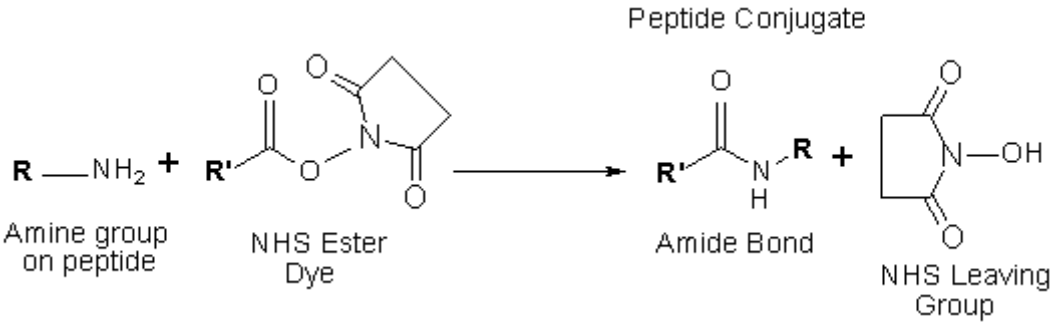

Figure 15. Diagram for NHS ester binding mechanism.

The most convenient and widely used functional group for the labelling of biological molecules is a primary amino group. This can be provided by the e-amino group of a lysine residue, or the free N-terminus of a peptide/protein. Alternatively, it is possible to introduce primary amine containing modifier groups during automated synthesis of, for example, oligonucleotides. Stable active esters of flora labelling species that may be stored as solid materials, in particular NHS ester, have been extensively used over many years for the acylation of such amino groups, as shown in the reaction schematic in figure 15.

Multiphoton microscopy

Multiphoton microscopy setup was as same as mentioned in chapter V. The laser source is sub-10-Femtosecond pulses and has spectra centered at 800nm with a full width at half-maximum (FWHM) of 133 nm. The Cy3.5 NHS ester fluorescent dye is excited at twice the wavelength used in ordinary fluorescence observations by absorbing the energy of two photons simultaneously. The excitation peak of Cy3.5 dye is around 550nm and emission peak is around 590nm as showed in figure 16. Since 500nm-550nm is within the bandwidth of our multiphoton imaging setup, with a 590nm emission filter Cy3.5 dye fluorescence signal can be acquired.

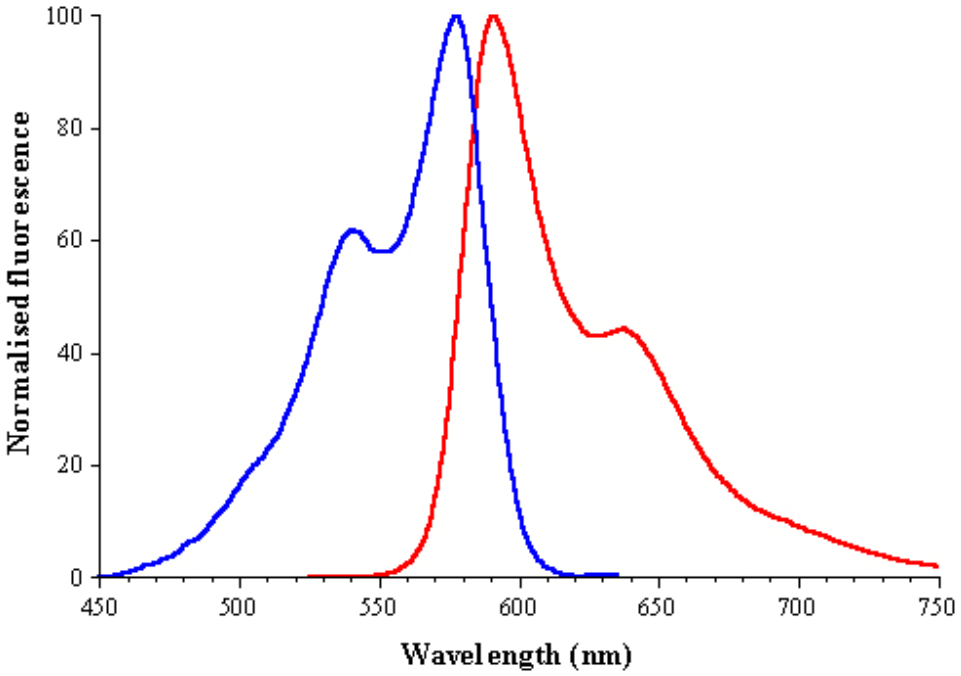

Figure 16. Excitation (blue line) and emission (red line) spectra of Cy3.5 dye.

Results and Discussion

Multiphoton microscopy study

Twenty minutes after 0.3 mM Cy3.5 NHS ester was added to the petri dish with a monolayer of ENU cells attached on the inner bottom, the cells were washed in MBSS and multiphoton microscopy images were collected (Fig. 17.). The dark spots in the middle of the cells are nucleolus inside cell nuclei. The high multiphoton signal (darker color) indicates high amino acid concentration. This is consistent with the fact the amino acid concentration in nucleolus is high since messenger RNA (mRNA) is translated from DNA (deoxyribonucleic acid) in the nucleolus of cells. The three white spots in figure 17 are dead ENU cells. Because Cy3.5 NHS ester does not label the dead cells, we can conclude that the dead cells lost the ability to transport the contrast agents through the cell membrane.

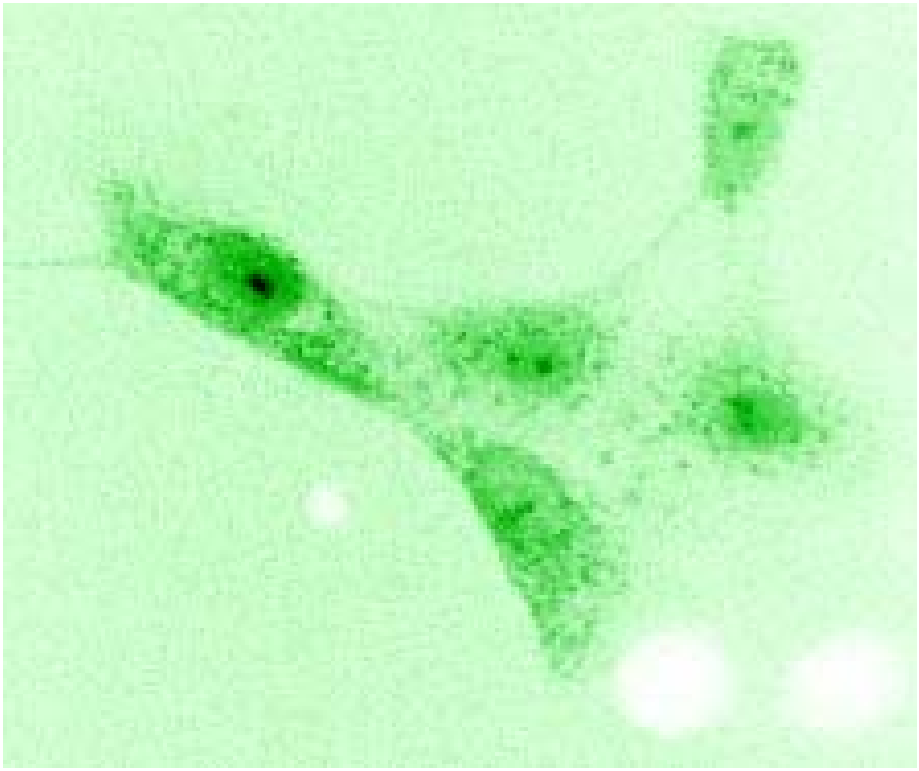

Figure 17. Multiphoton image of ENU cells. (40 Mag.)20 Minutes after 0.3mM Cy3.5 NHS ester Uptake.

Because the high nanometer resolution and high sensitivity, the multiphoton microscopy could be used to detect and monitor molecular level changes. Imaging of amino acid metabolism is difficult because of the optical characteristics of amino acid. It is invisible to the imaging systems which can only detect visible light wavelength. The fluorescence Cy3.5 NHS ester was used as a contrast agent for imaging amino acid metabolism successfully in this study. Due to the strong fluorescence signal emitted from Cy3.5 NHS ester, this contrast agent can be used for non invasive *in vivo* imaging study.

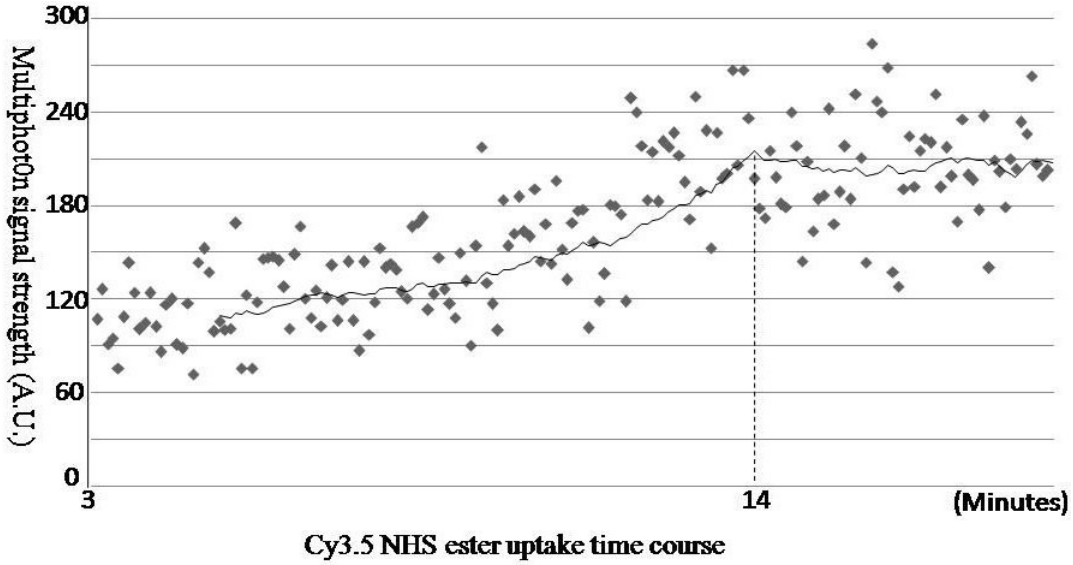

Figure 18. ENU cells dye uptake study.

Using Cy3.5 NHS ester by multiphoton microscopy. Changes of fluorescence signal strength within 20 minutes after adding 0.3 mM Cy3.5 NHS ester. X axis is the time course in minutes and the Y axis shows the fluorescence signal strength in arbitrary unit.

The time dependent ENU cells Cy3.5 NHS ester uptake is shown in figure 18. Three minutes after the ENU cells immersed in 0.3 mM Cy3.5 NHS ester with MBSS, a series of multiphoton microscopy images were taken at 10 seconds per frame for 20 minutes. Each data point is the average fluorescence signal strength per pixel per cell calculated from one multiphoton microscopy image contains about 10 cells at the specific time point. The data was collected from more than 120 images (images are not shown). The black line is average trend line for the corresponding data points. According to the

fluorescence signal strength recorded, the maximum uptake occurred at 14 minutes then the Cy3.5 NHS ester signal remained relatively constant.

In figure 19, concentration dependent ENU cells Cy3.5 NHS ester uptake is shown. Twenty minutes after the ENU cells immersed in 0.3, 0.2, 0.1 mM Cy3.5 NHS ester with MBSS, a series of multiphoton microscopy images were taken at 10 seconds per frame for 40 minutes. Same as in figure 18, each data point is the average fluorescence signal strength per pixel per cell calculated from one multiphoton microscopy image contains about 10 cells at the specific time point. The data was collected from more than 240 images (images are not shown). The black lines are trend lines for the corresponding data lines. From the data presented in figure 19, it shows that the multiphoton signal strength is not only related to amino acid concentrations distribution in the ENU cells but also related to the Cy3.5 NHS ester concentration used. So if this technique will be used to quantify the amino acid distribution, the contrast agent concentration must be considered.

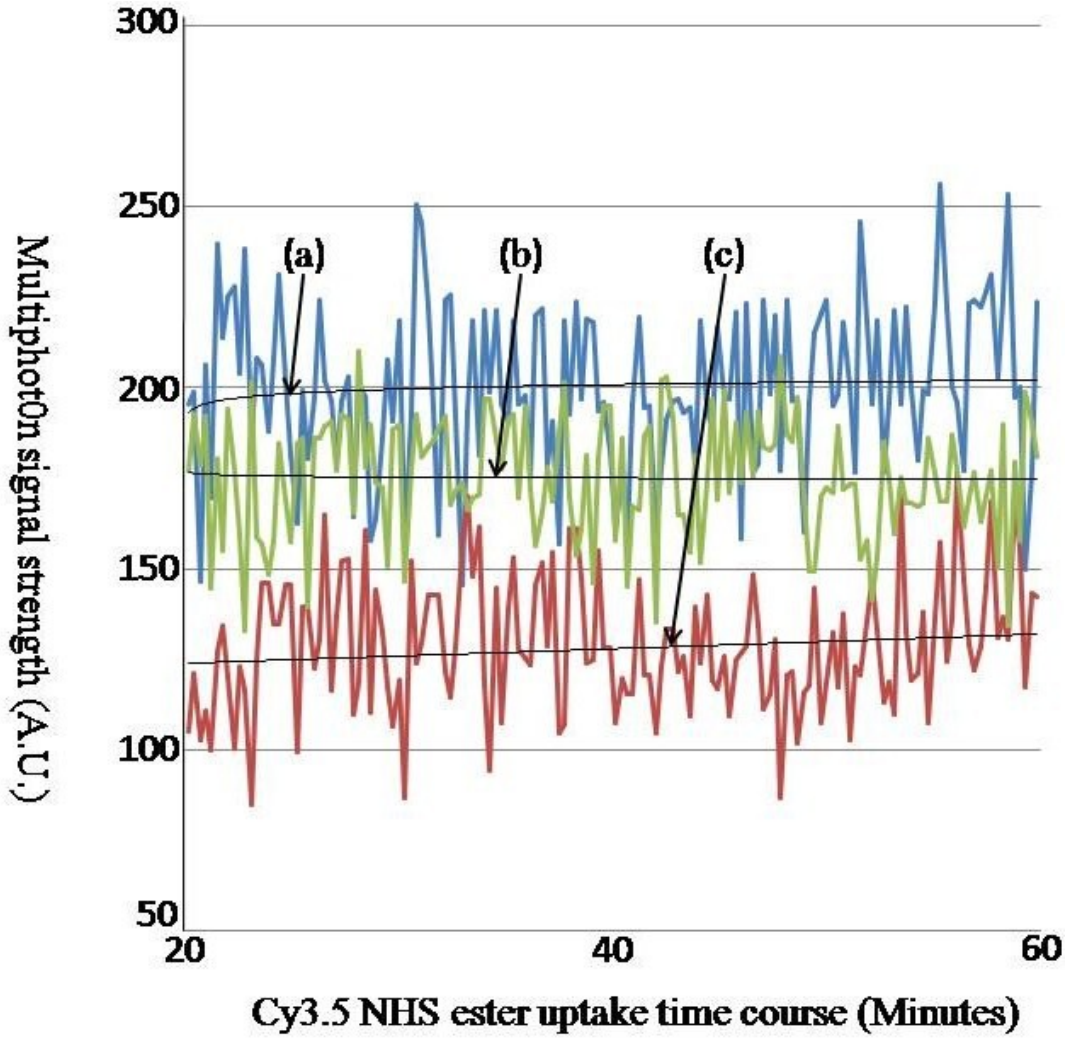

Figure 19. ENU cell free amino acid metabolism study.

Using Cy3.5 NHS ester with different concentrations. a) trend line for blue data line which was collected 20 minutes after ENU cell immersed in 0.3 mM Cy3.5 NHS ester; b) trend line for green data line which was collected 20 minutes after ENU cell immersed in 0.2 mM Cy3.5 NHS ester; c) trend line for green data line which was collected 20 minutes after ENU cell immersed in 0.1 mM Cy3.5 NHS ester.

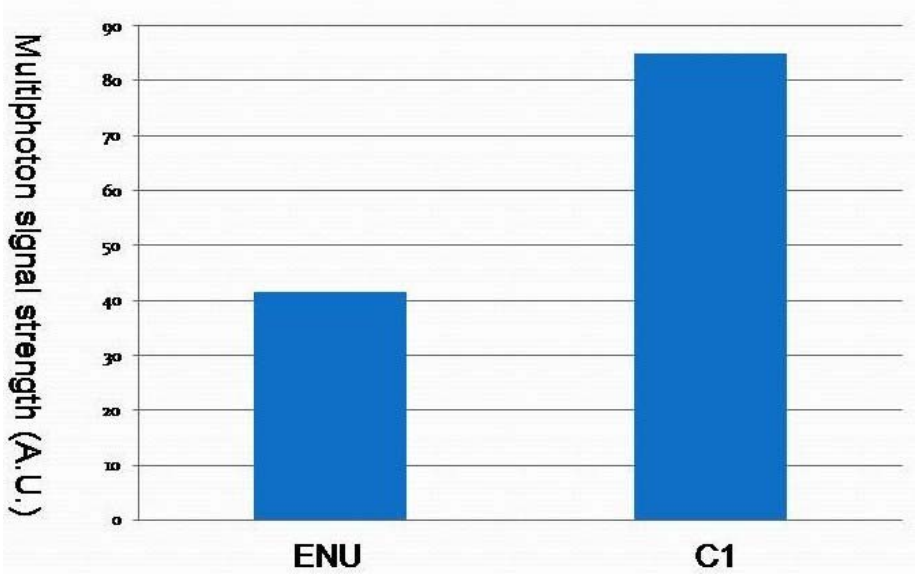

Figure 20. ENU cells and C1 astrocytes free amino acid metabolism study. Using Cy3.5 NHS ester. Images was collected 20 minutes after cells immersed in 0.1 mM Cy3.5 NHS ester.

In figure 20, ENU cells and immortalized murine C1 astrocytes Cy3.5 NHS ester uptake is shown. Twenty minutes after the cells immersed in 0.1 mM Cy3.5 NHS ester with MBSS, a series of multiphoton microscopy images were taken at 10 seconds per frame for 20 minutes. The y axis values are the average fluorescence signal strength per pixel per cell calculated from multiphoton microscopy images. The immortalized astrocytic line was developed from the cerebral cortex and brain stem of FVB/N mice infected with a retrovirus carrying the gene of the tsA58 T antigen by Dr. Wong's group in M.D. Anderson Cancer Center, University of Texas. From the data presented in figure 20, it shows that the ENU cell line has almost 2 times higher amino acid concentration

comparing to C1 astrocytes. This is due to the aggressive metabolism characteristic of the ENU tumor cells.

Conclusion

Our preliminary study showed that by implementing multiphoton microscopy using Cy3.5 NHS ester contrast agent, amino acid metabolism can be successfully studied in ENU cell culture. This method will at least lead to a relative concentration map of amino acid in cells which can be used as an indicator for protein metabolism in tumor. Non invasive *in vivo* imaging can be achieved by modifying the current multiphoton imaging device.

CHAPTER VII

SUMMARY AND CONCLUSION

In chapter II, M21 human melanoma tumor detection is successfully achieved by dual modality imaging method combining PAT and molecular fluorescence imaging. Nude mice M21 brain subcutaneous tumor angiogenesis was studied. A tumor-targeted NIR fluorescent contrast agent is used for the tumor detection. By employing coregistration of PAT and fluorescence imaging, the tumor location, the tumor angiogenesis, and even the brain surface histology structure of the nude mouse were revealed at the same time.

In chapter III and IV, non invasive functional molecular spectroscopic PAT imaging and quantification of brain tumor hemoglobin concentration and hemoglobin oxygenation through the intact skin and skull with satisfactory spatial resolution was presented. Tumor tissue hypoxia was observed at the same time when $\alpha_v\beta_3$ integrin distribution in brain tumor was measured as described in chapter IV. This study verified that spectroscopic PAT can be used to map point-by-point functional parameters and changes in tumor areas in the brain quantitatively with high spatial resolution. This will provide better understanding of tumor biology and potential use to new approaches for tumor therapy. This new technology can be further modified to accommodate real time detection of cancer in a minimally invasive manner. It could provide immediate

diagnostic and therapeutic information to the doctors to assist them on treatment plans even surgeries. This technology can help reduce morbidity and mortality of patients.

In chapter V, the preliminary study showed that by combining multiphoton microscopy and *in vivo* fluorescence imaging using 2-NBDG glucose analog, both the U87 tumor cell culture and *in vivo* nude mice brain tumor glucose metabolisms can be successfully evaluated. This demonstrates the possibilities to use multiphoton microscopy and fluorescence imaging technique with the assistance of fluorescence glucose analog to study glucose metabolism.

The monitoring of amino acid metabolism is very important for cancer detection, cancer development monitoring and therapy design. Chapter VI showed that by implementing multiphoton microscopy using Cy3.5 NHS ester contrast agent, tumor amino acid metabolism can be successfully studied in cell culture. This method will at least give you a relative concentration map of amino acid in cells. Non invasive *in vivo* imaging can be achieved by modifying the current multiphoton imaging setup.

REFERENCES

1. X. Wang, G. Ku, M. A. Wegiel, D. J. Bornhop, G. Stoica, and L.–H. Wang, Opt. Lett. **29** (7), 730 (2004).
2. X. Wang, Y. Xu, M. Xu, S. Yokoo, E. S. Fry, and L.–H. Wang, Med. Phy. **29** (12), 2799 (2002).
3. J. R. Lakowicz, in *Principles of Fluorescence Spectroscopy*, (Plenum Publishing, New York, USA, 1999).
4. W. Wang, S. Ke, and C. Li, Mole. Imag. **3** (4), 343 (2004).
5. S. Ke, X. Wen, and C. Li, Cancer Research **63**, 7870 (2003).
6. M. Xu, and L. V. Wang, IEEE T. Med. Imag. **21**,814 (2002).
7. P. Vaupel, and M. Hockel, Adv. Exp. Med. Biol. **510**, 45 (2003).
8. G.U. Dachs, G.M. Tozer, Eur. J. Cancer **36**, 1649 (2000).
9. G.L. Semenza, J. Appl. Physiol. **88**, 1474 (2000).
10. R. Hermans, P. Lambin, A. Van der Goten, W. Van den Bogaert, B. Verbist, C. Weltens, and P.R. Delaere, Radiother. Oncol. **53**, 105 (1999).
11. R. Hermans, M. Meijerink, W. Van den Bogaert, A. Rijnders, C. Weltens, and P. Lambin, Int. J. Radiat. Oncol. Biol. Phys. **57**, 1351 (2003).
12. H.M. Swartz and R.B. Clarkson, Phys. Med. Biol. **43**, 1957 (1998).
13. S. Ishida, H. Kumashiro, N. Tsuchihashi, T. Ogata, M. Ono, H. Kamada, and E. Yoshida, Phys. Med. Biol. **34**, 1317 (1989).
14. H.M. Swartz and T. Walczak, Adv. Exp. Med. Biol. **454**, 243 (1998).

15. D.F. Wilson, S. Vinogradov, L.W. Lo, and L. Huang, Adv. Exp. Med. Biol. **388**, 101 (1996).

16. C. Cheung, J.P. Culver, K. Takahashi, J.H. Greenberg, and A.G. Yodh, Phys. Med. Biol. **46**, 2053 (2001).

17. F. F. Jöbsis, Science **198**, 1264 (1977).

18. G. Ku, X. Wang, G. Stoica, and L.-H. Wang, Physi. in Med. and Biol. **49** (7), 1329 (2004).

19. G. Ku and L.-H. Wang, Opt. Lett. **30** (5), 507 (2005).

20. X. Wang, Y. Pang, G. Ku, X. Xie, G. Stoica, and L.-H. Wang, Nature Biotech. **21** (7), 803 (2003).

21. W. G. Zijlstra, A. Buursma, and O. W. V. Assendelft, in *Visible and Near Infrared Absorption Spectra of Human and Animal Hemoglobin, Determination and Application*, (VNU Science Press, The Netherlands, 2000).

22. B. Chance, E. Borer, A. Evans, G. Holtom, J. Kent, M. Maris, K. Mccully, J. Northrop, and M. Shinkwin, Ann. NY Acad. Sci. **551**, 1 (1988).

23. Y. Otsuki, H. Kubo, and S. Magari, Archives of Histo. and Cytol., **53** Suppl: 95 (1990).

24. X. Wang, Y. Pang, G. Ku, X. Xie, G. Stoica, and L.-H. Wang, Nature Biotech. **21** (7), 803 (2003).

25. G. Ku, X. Wang, G. Stoica, and L.-H. Wang, Phy. in Med. and Bio. **49** (7), 1329 (2004).

26. G. Ku and L.-H. Wang, Opt. Lett. **30** (5), 507 (2005).

27. P. Vaupel and M. Hockel, Adv. Exp. Med. Biol. **510**, 45 (2003).

28. G.U. Dachs and G.M. Tozer, Eur. J. Cancer **36**, 1649 (2000).

29. G.L. Semenza, J. Appl. Physiol. **88**, 1474 (2000).

30. W. G. Zijlstra, A. Buursma, and O. W. van Assendelft, in *Visible and Near Infrared Absorption Spectra of Human and Animal Hemoglobin, Determination and Application*, (VNU Science Press, The Netherlands, 2000).

31. S. Freeman, in *Biological Science*, (Prentice Hall, 2004), pp. 114-131.

32. R. A. Gatenby and R. J. Gillies, Nat. Rev. Cancer. **4**, 891 (2004).

33. C. J. Hoekstra, I. Paglianiti, O. S. Hoekstra, E. F. Smit, P. E. Postmus, G. J.J. Teule, A. A. Lammertsma, Eur. J. Nucl. Med. **27**, 731 (2000).

34. K. Yoshioka, H. Takahashi, T. Homma, M. Sato, B. O. Nemoto, H. Matsuoka, Biochim. Biophys. Acta. **5**, 1289 (1996).

35. C. H. Zou, Y. J. Wang, and Z. F. Shen, J. Biochem. Biophys. Methods **64**, 207 (2005).

36. R. G. O'Neil, L. Wu, and N. Mullani, Mol. Imaging Biol. **7**, 388 (2005).

37. P. G. Lloyd, C. D. Hardin, and M. Sturek, Physiol. Res. **48**, 401 (1999).

38. A.M. Larson and A. T. Yeh, Opt. Lett. **31**, 1681 (2006).

39. W. R. Zipfel, R. M. Williams, and W. W. Webb, Nature Biotech. **21**, 1369 (2003).

40. G. L. Blackburn, J. P. Grant, and V. R. Young, in *Amino Acids: Metabolism and Medical Applications*, (John Wright PSG, 1983), pp. 1-2.

41. N. F. Cheville, in *Introduction to Veterinary Pathology*, (Iowa State Univ. Press, Iowa, USA, 1988), pp. 521-521.

42. G. L. Blackburn, J. P. Grant, J.P., and V. R. Young, in *Amino Acids: Metabolism and Medical Applications*, (John Wright PSG, Boston, USA, 1983), pp. 213-214.

43. D. A. Bender, in *Acid Metabolism*, (John Wiley & Sons, NJ, USA, 1985), pp. 111-112.

VITA

Xueyi Xie received his B.S. in applied chemistry from Qingdao University in July 1997 and his M.S. in computer science from University of North Texas in 2002. He later researched under Dr. Gheorghe Stoica of Texas A&M University from the spring of 2003. His research was mainly focused on the small animal malignant tumor physiology using noninvasive *in vivo* functional imaging technologies.

Mr. Xie may be reached at 8515 Parkvilla Dr., Apt #109E, Mountain Iron, MN 55768. His email address is thomasxie@gmail.com.